scientific reports

Check for updates

OPEN

Synergistic effects of human umbilical cord mesenchymal stem cells/neural stem cells and epidural electrical stimulation on spinal cord injury rehabilitation

Zhiping Mu[1,4], Jiaodi Qin[2,4], Xiaohua Zhou[3,4] & Kunzheng Wang[1]✉

Spinal cord injury (SCI) is a severe neurological condition marked by a complex pathology leading to irreversible functional loss, which current treatments fail to improve. Epidural electrical stimulation (EES) shows promise in alleviating pathological pain, regulating hemodynamic disturbances, and enhancing motor function by modulating residual interneurons in the lower spinal cord. Cell transplantation (CT), especially using human umbilical cord mesenchymal stem cells (hUCMSCs) and neural stem cells (NSCs), has significantly improved sensory and motor recovery in SCI. However, the limitations of single treatments have driven the exploration of a multifaceted strategy, combining various modalities to optimize recovery at different stages. To comprehensively investigate the effectiveness of in situ transplantation of hUCMSCs/NSCs combined with subacute epidural electrical stimulation in a murine spinal cord crush injury model, providing valuable references for future animal studies and clinical research. In this study, we first examined neural stem cell changes via mRNA sequencing in an in vitro Transwell co-culture model. We then explored cell interaction mechanisms using proliferation assays, differentiation assays, and neuron complexity analysis. For animal experiments, 40 C57BL/6 mice were assigned to four groups (Injury/EES/CT/Combination). Histological evaluations employed HE and immunofluorescence staining, while electrophysiological and behavioral tests assessed motor recovery. Quantitative data were reported as mean ± standard error, with statistical analyses performed using GraphPad Prism and SPSS. Initially, we found that NSCs in the in vitro co-culture model showed a unique expression profile of differentially expressed genes (DEGs) compared to controls. GO/KEGG analysis indicated these DEGs were mainly linked to cell differentiation and growth factor secretion pathways. Neuronal and astrocytic markers further confirmed enhanced NSC differentiation and neuronal maturation in the co-culture model. In vivo, live imaging and human nuclei immunofluorescence staining revealed that transplanted cells persisted for some time post-transplantation. Histological analysis showed that during acute inflammation, both the stem cell and combined therapy groups significantly inhibited microglial polarization. In the chronic phase, these groups reduced fibrotic scar formation and encouraged astrocytic bridging. Behavioral tests, including swimming and gait analysis, demonstrated that combined CT and EES therapy was more effective than either treatment alone. In summary, the combined therapy offers a promising approach for spinal cord injury treatment, providing superior outcomes over individual treatments. Our findings underscore the potential of a combined treatment approach utilizing stem cells transplantation and EES as an effective strategy for the comprehensive management of spinal cord crush injury in mice. This integrated approach holds promise for enhancing functional recovery and improving the quality of life for individuals with spinal cord injury (SCI).

Keywords Spinal cord stimulation, Human umbilical cord mesenchymal cell, Neural stem cell, Epidural electrical stimulation, Combinatorial therapy

[1]Department of Bone and Joint Surgery, The Second Affiliated Hospital of Medical College, Xi'an Jiaotong University, Xi'an 710004, Shaanxi, People's Republic of China. [2]First Clinical Institute, Chongqing Medical University, Chongqing 400016, People's Republic of China. [3]Chongqing Shizhu Tujia Autonomous County Traditional Chinese

Medicine Hospital, Chongqing 409199, People's Republic of China. [4]Zhiping Mu, Jiaodi Qin and Xiaohua Zhou have contributed equally to this work and share first authorship. ✉email: wkzh1955@163.com

Spinal cord injury (SCI) is a significant neurological disorder that can lead to enduring alterations in spinal cord functionality[1]. The substantial morbidity, disability, and financial implications linked to spinal cord injuries impose a noteworthy physical, psychological, and financial burden on both patients and their families[2]. Based on statistical data, the worldwide prevalence of spinal cord injury (SCI) is estimated to range from 11 to 16 cases per 100,000 individuals per year, with falls and traffic accidents identified as the predominant etiologies[3]. Primary injuries often lead to spinal cord edema, hemorrhage, and microcirculation disorders. A series of secondary injuries can further expand the damage zone and cause neurological dysfunction[4]. Current treatment methods for SCI include surgical intervention, pharmacotherapy, and rehabilitation therapy[5]; however, these approaches fail to effectively repair SCI. Among the existing treatment options, early decompression surgery[6] and corticosteroid pulse therapy[7] have shown poor outcomes and are prone to a variety of severe complications. Rehabilitation therapy is costly and only allows for limited functional recovery[8], thus there is an urgent need to find and establish effective post-injury spinal cord repair strategies. Research in the field of spinal cord injury repair is currently centered on enhancing the regenerative capacity of injured axons, improving the spinal microenvironment, and increasing the plasticity of residual motor-related interneurons.

Human umbilical cord mesenchymal stem cells (hUCMSCs) have been identified as a promising reparative method for spinal cord injury (SCI) due to their plentiful source, low ethical restrictions, and powerful regenerative capabilities. hUCMSCs are widely available and can be obtained through non-invasive methods. These cells exhibit the benefits of multilineage differentiation, rapid proliferation, straightforward extraction, and prolonged post-transplantation survival, rendering them promising candidates for central nervous system transplantation[9]. The investigators found that transplanting hUCMSCs into the epicenter of a spinal cord injury on the 10th day following injury resulted in a reduction in inflammation-related cytokines IL-7, IFN-γ and TNF-α, There is a greater expression of anti-inflammatory cytokines IL-4 and IL-13 at the site of injury, and a greater activation of M2 macrophages[10]. Rats subjected to treatment with human umbilical cord mesenchymal stem cell-derived extracellular vesicles (hUCMSCs-EVs) demonstrated notable enhancements in motor function and reductions in necrosis, nuclear pyknosis, and cavity formation[11]. In the realm of tissue engineering, human umbilical cord mesenchymal stem cells are commonly employed as optimal seed cells. Twenty participants with acute complete cervical injuries received collagen scaffolds containing neonatal hUCMSCs as part of a preliminary clinical trial. The research observed enhancements in American Spinal Injury Association (ASIA) scores and activities of daily living scores. Additionally, MRI results showed the development of new nerve fiber connections, whereas diffusion tensor imaging (DTI) showed the return of electrophysiological function[12]. Numerous preclinical studies have demonstrated regenerative potential of transplanted neural stem cells (NSCs) in animal models of spinal cord injury.[13]. These therapeutic effects are mediated by paracrine signaling pathways and direct neuronal differentiation, ultimately facilitating the reestablishment of synaptic connections and neural circuitry[14]. Cheng et al. have conducted studies on the optimal timing of neural stem cell transplantation, revealing that transplantation during the subacute phase yields significantly greater efficacy compared to transplantation during the chronic phase in animal models. This study indicates that the timely transplantation of NSCs may provide enhanced advantages for individuals suffering from spinal cord injuries[15]. Multiple clinical Phase II studies have demonstrated the safety and efficacy of Neural Stem Cell (NSC) treatment over a period of 1–2 years, showing promising results in enhancing patient behavioral recovery[16,17].

In recent years, there has been a significant increase in the use of physical therapies, particularly spinal cord stimulation (SCS), for the management of spinal cord injuries, attributed to their precise targeting and limited systemic adverse effects. Epidural electrical stimulation (EES) is a minimally invasive surgical procedure involving the insertion of electrodes above the dorsal aspect of the spinal dura mater, thereby influencing the excitability and operational state of the spinal network[18]. Originally employed primarily for the treatment of refractory pain conditions, the EES method was first introduced by Melzack and Wall in 1965[19], who proposed the theory of "pain gate control." This theory posits that electrical stimulation suppresses the activity of Aβ and C afferent sensory fibers in the spinal cord, thereby impeding the transmission of pain signals to the brain. As researchers gained a more comprehensive comprehension of sensory dermatomes and the induction of paresthesia coverage in the region of pain, coupled with advancements in electrode technology capable of spanning a wider array of segments with multiple contacts and columns, EES emerged as a prevalent method for managing chronic pain. A preliminary intervention involving Epidural Electrical Stimulation (EES) therapy in individuals with chronic spinal cord injury yielded reductions in muscle spasticity and partial restoration of movement in the knees and ankles[20]. In a study conducted by Joshi et al.[21], 14 individuals with chronic, severe cervical spinal cord injury (SCI), all of whom had implanted neurostimulators, participated in assessments. The study demonstrated overall improvements in lower spine posture and a reduction in the need for trunk assistance. In addition to its role in facilitating the recovery of motor functions, EES has emerged as a promising and efficacious therapeutic approach for addressing autonomic dysfunctions that arise subsequent to spinal cord injury[22]. Meanwhile, EES has demonstrated efficacy in enhancing cardiovascular hemodynamics[23], reinstating regular respiratory patterns[24], mitigating disruptions in gastrointestinal function, and alleviating urinary retention[25].

In our study, we established four experimental groups: the CT (cell transplantation) group, which received a transplantation of hUCMSCs/NSCs; the EES group, which underwent epidural electrical stimulation; the combined treatment group, which received both of the aforementioned treatments; and the control group, which did not receive any form of treatment. A singular intervention has demonstrated limited effectiveness in addressing the varied characteristics of spinal cord injury throughout different stages of treatment. Thus, we propose a novel sequential treatment approach for spinal cord injury, involving the transplantation of hUCMSCs/NSCs in the acute phase to modulate the local injury microenvironment, and the provision of epidural electrical

stimulation during the subacute and chronic phases to regulate axon regeneration ability. In order to better understand the interplay between neural stem cells and mesenchymal stem cells in co-culture systems, a co-culture model was developed. NSCs were cultivated in the lower compartment of Transwell chambers, with human umbilical cord mesenchymal stem cells in the upper compartment. Following a 14-day in vitro co-cultivation period, neural stem cells from the lower compartment were harvested for mRNA transcriptome sequencing and subsequent bioinformatics scrutiny. This research examined the impact of co-administration hUCMSCs/NSCs and EES on spinal cord injury (SCI) repair, as well as the underlying mechanism, to provide insight into a potential novel therapeutic approach for SCI.

Materials and methods

Extraction and library construction

The purity and integrity of the RNA samples were evaluated through the 260/280 ratio measurement on a NanoDrop ND-1000 and the Bioanalyzer 2100, respectively. A RIN value exceeding 7.0 was established as the criterion for RNA integrity. Afterwards, 1 g of total RNA was isolated with Dynabeads Oligo (dT)25–61,005 with two rounds of purification. In the magnesium RNA Fragmentation Module, the poly(A)RNA was fragmented for 5 to 7 min at 94 °C prior to reverse transcription to form cDNA. A-bases were added to each blunt end of each strand to facilitate ligation. The adapters had T-base overhangs to allow for binding with DNA fragments containing A-tails. AMPure XP beads (Beckman Coulter, California, USA) were used to select size after ligation of single-index or dual-index adapters to fragments. The heat-labile UDG enzyme was used to label second-stranded DNAs for PCR amplification. The mean insert size of the resultant cDNA library was found to be 300 ± 50 base pairs. Following amplification of the cDNA library, paired-end sequencing (PE150) was performed with 2×150-bp reads on a NovaSeqTM6000 platform according to manufacturer directions.

The utilization of bioinformatics tools for the analysis of RNA-seq data

The reads with adapter contamination and low-quality bases were eliminated using the Fastp software with default settings. StringTie was then used to assemble the mapped reads with default settings. Following the merging of all transcriptomes from the samples, gffcompare was utilized to reconstruct a comprehensive transcriptome. We then used StringTie to calculate mRNA expression levels using FPKM (FPKM = [total_exon_fragments/mapped_reads (millions) × exon_length (kB)]). Using edgeR, differentially expressed mRNAs were identified with a fold change greater than 2 or less than 0.5, and a P value less than 0.05 from a parametric F test comparing nested linear models.

Animal housing

This study utilized adult female C57BL/6 mice weighted 20 g, all of which were purchased from Beijing Vital River. All animals were acclimated for at least one week at Animal Center (LAC) of Xi'an Jiaotong University (XJTU) before the start of the experiment. The temperature in the animal room was maintained between 26 ℃, and the humidity was kept at 50%. The light–dark cycle was 12 h of light followed by 12 h of darkness. All animals received standard laboratory chow and tap water, and were housed according to the institution's standard operating procedures. In our study, the experimental unit was defined as a single animal. Each experimental group consisted of female mice from the same litter, which were randomly assigned to different treatment groups. Each treatment group received specific intervention measures, while the control group underwent spinal cord injury to create the injury model. All animals were randomly grouped before the start of the experiment to ensure similar baseline characteristics between groups. Additionally, each group of animals was housed in separate cages to avoid any inter-group interactions. In our study, we allocated 10 experimental units to each group, resulting in a total of 40 animals across all treatment and control groups. The total number of animals used in the study was 40, which includes the experimental animals and excluded due to health issues or experimental complications. Experimental units were randomly allocated to control and treatment groups. We used a computer-generated random number sequence to create the randomization sequence. The sample size for each group was determined based on power analysis to ensure that the study had sufficient statistical power to detect a meaningful effect of the treatment. Inclusion and exclusion criteria for animals were established a priori. Additionally, animals were continuously monitored throughout the experiment. Any animal exhibiting significant weight loss, dragging and friction injuries to the lower limbs, or severe conditions such as bedsores or gangrene was excluded from the study. Injury Group: Two animals were excluded; one due to an aggravated infection following prolonged dragging injury of the lower limbs, which ultimately resulted in its elimination, and another due to a serious urinary tract infection. In the EES group, one animal experienced electrode detachment and damage. The remaining animals and data points were included. This research work has been reported in line with the ARRIVE guidelines 2.0.

Mice model of spinal cord crush injury

Experimental procedures were carried out according to the guidelines established by the Animal Welfare Committees of Xi'an Jiaotong University in Xi'an, China. Female C57BL/6 mice weighing between 20 and 23 g were used in the experiments. Using the Flexible Veterinary Anesthesia Machine-Wall Mount (RWD R640, China), mice were anesthetized with isoflurane (2.5% during induction, 1.5% throughout the procedure). We performed a laminectomy at the T10 level in order to gain access to the spinal cord. No. 5 Dumont forceps (Fine Science Tools) were used to compress the spinal cord for 3 s. Afterwards, the wound was plugged with a hemostatic sponge (Roeko, China). All wounds were irrigated with a sodium chloride solution and subsequently sutured in layers. To aid in urination, bladder compression was performed daily until the mice were humanely euthanized. During the initial three days post-operation, the administered dosage of amoxicillin (Aomei, China) was 0.25 mg/mL in oral suspension to prevent infection.

Implantation of EES electrode and therapeutic electrical stimulation

Each experimental animal underwent the implantation of an epidural electrode as the stimulating electrode, with all devices being sterilized before the implantation procedure. Firstly, one week after the initial injury, the previous surgical site is reopened using a scalpel. Subsequently, laminectomy is performed at the caudal end of the original injury site (T12), followed by insertion of an epidural electrode (Kedou, China) to estimate the contact point at the predicted injury location. A 3 − 0 silk suture is then used to secure the electrode's side ear to the paraspinal muscles. The electrode connector is routed through a subcutaneous tunnel and secured to the back to prevent the animal from biting it. An 3 − 0 nylon suture was used to close the injury site and muscle fascia, followed by tissue adhesive glue (3 M, US) to close the skin. After surgery, the mice were allowed to recover on a heating pad before being returned to individual cages maintained on a 12-h light/12-h dark cycle, ensuring that lights were not used and researchers and technicians refrained from entering the mouse room during the dark phase. The environmental temperatures were controlled within 65–75°F (~ 18–23 °C) with 40–60% humidity. The commonly utilized clinical therapeutic electrical stimulation protocol, consisting of continuous 10 Hz, biphasic pulses of 100 μs duration at 5–10 V, was employed as the stimulation paradigm. In the EES group, the lead extension connectors were connected to both the waveform generator and the amplifier (Tektronix AFG3051C, US). The platinum leads were used to deliver electrical stimulation to the injured spinal cord for a duration of 20 min per day, consistently over a period of 7 weeks.

Cell sources for human mesenchymal stem cells

In this study, human umbilical cord-derived mesenchymal stem cells (hUC-MSCs) were utilized, provided by Tianjin Changhe Biotechnology Co., Ltd. Prior to shipment, the cells underwent a series of quality control assessments conducted by the company's inspection facility. Following successful release, the cells were transported under a low-temperature dry ice cold chain. Upon receipt, the cell morphology was inspected, and the cells were subsequently stored in liquid nitrogen for future use. All procedures were conducted in accordance with relevant ethical guidelines and operational regulations.

Isolation and culture of rat embryonic cortical NSCs

Mouse embryonic cortical neural stem cells (NSCs) were obtained and cultured following the protocol outlined by Reynolds[26] and Weiss[27], with minor adjustments. Pregnant female C57 mice at 13.5 days of gestation were anesthetized with isoflurane and euthanized via cervical dislocation in a sterile environment. Subsequently, the embryos were extracted, the bilateral cerebral cortices were dissected, and the meninges were removed. The embryos were dissected to isolate the bilateral cerebral cortices and remove the meninges. The tissue was then finely minced using ophthalmic scissors, followed by digestion in a solution containing 2 mg/mL papain and 10 U/mL DNase I in DMEM medium for 10–20 min. After digestion, the cell suspension was filtered through a 40 μm cell strainer to eliminate any remaining tissue fragments. The filtered suspension was subsequently combined with growth medium and seeded into T-75 culture flasks for further cultivation. The culture medium was refreshed by replacing half of the volume every other day, and cell passaging was performed using Accutase cell digestion solution every 7 days. Cells between 2 and 4 passages were utilized for subsequent experiments. Prior to experimentation, NSCs were digested and plated onto culture dishes precoated with 0.01% poly-L-lysine and 2 μg/mL laminin to facilitate growth in a monolayer rather than as neurospheres for enhanced visibility. Additionally, NSCs were transitioned to differentiation medium prior to conducting differentiation assays.

Process of cell transplantation

The chronically injured mice were anesthetized with inhalation of isoflurane prior to the reopening of the laminectomy site. The laminectomy site at the T_9/T_{10} level was reopened in chronically injured mice, who were receiving an injection of NSCs and hUCMSCs (3 μl, 300,000 cells). The cells were transplanted into three equal parts at three separate locations along the midline of the spinal cord: at the rostral (headward) end, the caudal (tailward) end, and directly at the site of the lesion. For this procedure, a Hamilton syringe with a 10 μl capacity was used, equipped with a 32-gauge needle that was 0.5 inches long and had a 30° beveled tip. This setup was utilized to inject 3 μl of cell suspension at each site, which contained 100,000 cells per μl, leading to a total of 300,000 cells being injected at each of the three equidistant points. These points were situated at the center of the lesion and 1 mm both rostral and caudal to the lesion's epicenter[28]. In the Injury and EES groups, PBS solution was injected following the aforementioned procedure, whereas in the CT and Combination groups, cells were administered. The infusion of PBS or cells was conducted at a controlled rate of 1 μl per minute using a microinjector pump (Stoelting, Wood Dale, IL, USA). For maximum protection against cellular backflow or regurgitation, the needle was left in place for an additional five minutes after the injection. This step was crucial to ensure that the transplanted cells remained at the intended injection sites within the spinal cord. After the injection was completed, the injection sites could be clearly observed on the surface of the spinal cord. Once there was no active bleeding or spinal cord edema observed, the wound was closed. This step was crucial to ensure that the injection process did not cause any additional damage to the spinal cord and provided favorable conditions for wound healing.

Immunocytochemistry

Immunocytochemistry (ICC) was conducted as follows: The cultures were washed twice with a blocking solution (QuickBlock™ Blocking Buffer,P0260, Beyotime) and then primary antibodies were incubated overnight, and the secondary antibodies were incubated for one hour.. To visualize the nuclei, DAPI (ThermoFisher D3571) was added for 10 min before washing the cells three times with PBST. The antibodies used in this process included anti-GFAP (glial fibrillary acid protein, ab7260; 1:500; Abcam) for detecting astrocytes and anti-tubulin βIII (ab78078, Abcam, 1:500) for identifying newly formed neuronal axons. The cell culture plates were then

incubated with secondary antibodies conjugated to Alexa Fluor 488 for rabbit antibodies (ab150077; 1:1000; Abcam) and Alexa Fluor 555 for mouse antibodies (ab150118; 1:1000; Abcam).

EdU proliferation assay for NSCs

Using an EdU detection kit (C0075L, Beyotime), NSCs were tested for their proliferation ability. Firstly, the neurons were incubated in the dark at 37 °C for 2 h with a 10 M buffer containing 5-ethynyl-2'-deoxyuridine (EdU). After the incubation period, the EdU working solution was aspirated, and the cells were washed to remove any unincorporated EdU. Subsequently, the cells were fixed at room temperature to preserve the incorporated EdU within the DNA for further detection and analysis. A 0.3% Triton X-100-PBS solution was applied for 10 min after the fixative was removed from the cells. After the permeabilization solution was aspirated, the cells were washed twice with PBS to remove any remaining permeabilization reagents. Hoechst 33,342, a nucleic acid stain that binds to DNA and allows visualization of the cell nuclei, was then added to the cells. During the incubation, Hoechst 33,342 bound to DNA for 10 min at room temperature. After the Hoechst 33,342 incubation, the solution was aspirated, and the cells were washed again with PBS to remove any excess Hoechst 33,342. Finally, images of the cells were captured for analysis, typically using a fluorescence microscope to visualize the stained nuclei.

EdU Proliferation Assay for NSCs.

Morphological analysis

In the study, the complexity of neuronal branches and networks was assessed by measuring the number and length of neurites. As previously described in references[29], morphological analyses, including Sholl analysis, were conducted. The dendrites and axons, which are the neuronal processes, of differentiated neurons were manually counted. In each experiment, five microphotographs were randomly obtained from each well and subjected to analysis using ImageJ software (NIH, Bethesda, USA). A total of 40 neurons from each group were included in the statistical analysis. The Simple Neurite Tracer plugin was employed for the semi-automatic tracing of neurons. After delineating the morphology of the neurons, concentric circles with a radius increment of 20 μm were drawn from the soma as the center, extending up to 240 μm. The number of intersections between these concentric circles and the neuronal processes was recorded.

Functional studies

Basso mouse scale locomotor score

BMS assessments were performed on all cohorts of mice at various time intervals following surgical procedures, specifically on days − 1, 1, 3, 7, 14, 21, 28, 35, 42,49 and 56. Prior to assessment, the mice's bladders were voided completely. The BMS (Basso Mouse Scale) test is a method used to assess the functional recovery of lower limbs in mice after spinal cord injury. It involves scoring the hindlimb movements of the mouse on a scale from zero to nine, with higher scores indicating better motor function. For the test, the hindlimb movements of the mouse are visually observed within an open field chamber measuring 100 cm*70 cm for a duration of 5 min. This open field environment allows for the assessment of the mouse's mobility and motor function without the constraints of a confined space. Additionally, the bottom of the open field chamber is made of a non-slip material to prevent any abnormal hindlimb movements that could be caused by a excessively smooth frictional interface. This ensures that the mouse's movements are not artificially influenced by the chamber floor, allowing for a more accurate assessment of their motor function. The observer looks for specific motor behaviors, such as limb placement, weight support, and coordination of movements, to assign an appropriate score. This test is a valuable tool in research settings to evaluate the efficacy of potential therapeutic interventions for spinal cord injury. The mice were allowed to freely move in an open space, while two blinded researchers independently conducted scoring, documenting the average scores for both the left and right sides of the mice. The evaluation focused on ankle joint movement, plantar placement, plantar stepping, and movement coordination[30].

Louisville swim scale

A transparent chamber with dimensions of 60 cm in length, 33 cm in width, and 38 cm in depth was used as a swimming pool. It was equipped with a ramp on one side, which was constructed from an acrylic plate combined with a 5-mm-thick layer of chloroprene rubber. This setup allowed for the observation of swimming behavior and provided a surface with sufficient grip for the animals to navigate into and out of the water[31]. The pool was filled with warm tap water to a depth of 30 cm, with a consistent temperature range of 28–30 °C. Mice underwent training to swim across the pool and reach the ramp for exit twice prior to the final assessment, which took place 8 weeks after the injury.

In this study, hindlimb movement and alternation, forelimb dependency, trunk stability and body angle were measured via Louisville Swim Scale (LSS) scoring sheets with 0 to 17 points.

Catwalk gait analysis system

In order to quantify locomotor recovery in mice, the CatWalk XT system by Noldus (version 10.6, Noldus, Netherlands) was used. The CatWalk XT 10.6 Reference Manual and a previous study were consulted for guidance[31,32]. The footprints of 8-week-old mice were captured by a camera placed beneath the glass, as they walked voluntarily on a glass walkway illuminated by a fluorescent light in the dark. Before the test, mice undergo 2–3 training sessions where food is placed at the end of the runway to encourage them to complete the task. This pre-training familiarizes the mice with the setup and the expected behavior, which typically guarantees their performance during the actual test. The use of food as a reward helps to motivate the mice and can enhance their engagement in the experiment. Eight weeks post-injury, we allowed the mice to walk voluntarily on a glass walkway illuminated by fluorescent light in a darkened environment. A camera positioned

below the glass surface recorded the footprints of the mice. The accompanying software, was used to analyze the recorded footage, calculating a range of statistics related to the mice's locomotion. These statistics included the dimensions of each stride, the total time taken to walk a certain distance, the overall distance traveled, and the coordination between individual footprints. This analysis provides a detailed quantitative assessment of the mice's walking pattern and gait, which is essential for evaluating motor function and potential changes over time or in response to various treatments. Each animal was required to complete three consecutive compliant runs at each designated time point to ensure consistency and reliability in the data collected.

Electrophysiological detection

Anesthetized with isoflurane anesthesia, the mice were then depilated using depilatory cream on the skull, back, and both lower legs thereafter. The stimulating electrode was placed on the skull, corresponding to the primary motor cortex in the left and right brain regions. Recording electrodes were positioned in the bilateral gastrocnemius muscle complex, and a ground electrode was attached to the dorsal skin. The muscle evoked potentials (MEPs) of each mouse were recorded three times. The stimulation protocol was conducted according to the built-in program of the electrophysiological device (YRKJ-G System, Zhuhai, China), consisting of five stimulation waves with an intensity of 5 mA each[33].

Tissue harvesting

The mice were induced into a state of complete anesthesia through excessive isoflurane inhalation.

Perfusion of PBS at pH 7.4 and 4% paraformaldehyde in 0.1 M PBS followed anesthesia. After the perfusion, the spinal cords were surgically removed and then post-fixed in the same fixative solution overnight. The next day, the spinal cords were submerged in a solution of 30% sucrose in PBS, and the dura mater was removed using instruments under a stereomicroscope. For subsequent analysis, a segment of the spinal cord containing the injury site at the thoracic level was meticulously dissected and embedded in optimal cutting temperature compound (OCT). The frozen samples were then sectioned into 10 μm slices using a cryostat microtome (CM 3050S Leica).

Immunohistochemistry

The 10-μm-thick longitudinal frozen sections of the spinal cord samples were permeabilized and blocked by blocking solution (P0260, Beyotime) for an hour at room temperature prior to incubation overnight with primary antibodies: rabbit anti-PDGFR-β (MA5-33,050, Abcam, 1:200), mouse anti-GFAP (14–9892-82, Thermo Fisher, 1:500), mouse anti-CD68 (14–0688-82, Thermo Fisher, 1:200), rabbit anti-Arginase 1 (PA5-29,645, Thermo Fisher, 1:200), rabbit anti-iNOS (PA1-036, Thermo Fisher, 1:200), incubated overnight in a solution composed of 5% bovine serum albumin (BSA) within a 0.25% Triton X-100 solution, all diluted in 0.1 M Tris-Buffered Saline with Tween 20 (TBST). The next day, the slides were washed with 0.1 M Tris-Buffered Saline with Tween 20 (TBST), and the antigen/antibody complexes were incubated with either Goat anti-rabbit Cy3 (Abcam, 1:500), Goat anti-mouse Alexa Fluor 488 (Abcam, 1:500), or Goat anti-rabbit Alexa Fluor-488 (Abcam, 1:500). After an hour of incubation, the slides were washed three times in TBST.

Hematoxylin–eosin staining

Hematoxylin–Eosin (HE) staining was employed to evaluate the bladder wall thickness of the animals in each group at eight weeks post-injury. By assessing the bladder wall thickness, we aimed to reflect the extent of urinary retention. Bladder samples were fixed in paraffin, sectioned, and stained using an HE staining kit (Solarbio, Beijing, China). Subsequently, the sections were examined under an optical microscope (IX73, Olympus, Tokyo, Japan). The thickness of the bladder wall in each group was quantified using ImageJ software to compare the outcomes between the two groups.

Data analysis

The data normality was evaluated with the Kolmogorov–Smirnov test, and the variance homogeneity was evaluated using Levene's test. If the data were normally distributed and the variance was homogeneous, we performed one-way ANOVA followed by the post hoc Tukey's test. If the data were not normally distributed or variance homogeneity was not met, the Kruskal–Wallis test was performed followed by the post hoc Mann–Whitney U test.

Results

Identification of DEGs in the CTL and Coculture groups

To enhance comprehension of the reciprocal interaction between NSCs and hUCMSCs in co-culture systems, a Transwell co-culture model was devised. NSCs were cultivated in the lower compartment of Transwell chambers, with hUCMSCs in the upper compartment. After a 14-day period of in vitro co-cultivation, NSCs from the lower compartment were collected for mRNA transcriptome sequencing. The resulting data were then subjected to bioinformatics analysis to identify genes that are associated with the observed cellular processes or characteristics. In the heatmap, the top 100 DEGs were highlighted, as depicted in Fig. 1A. Using a cutoff of $P < 0.05$ and a fold change threshold of $|\log FC| > 1$, a total of 2014 DEGs were identified between the Coculture and control groups, with 1127 genes being upregulated and 887 genes downregulated (Fig. 1B). A volcano plot was utilized to visually illustrate these DEGs, as shown in Fig. 1C. These findings indicate that the co-culture model with human umbilical cord mesenchymal stem cells (hUCMSCs) has a significant impact on NSCs when compared to the standard in vitro culture model of normal NSCs.

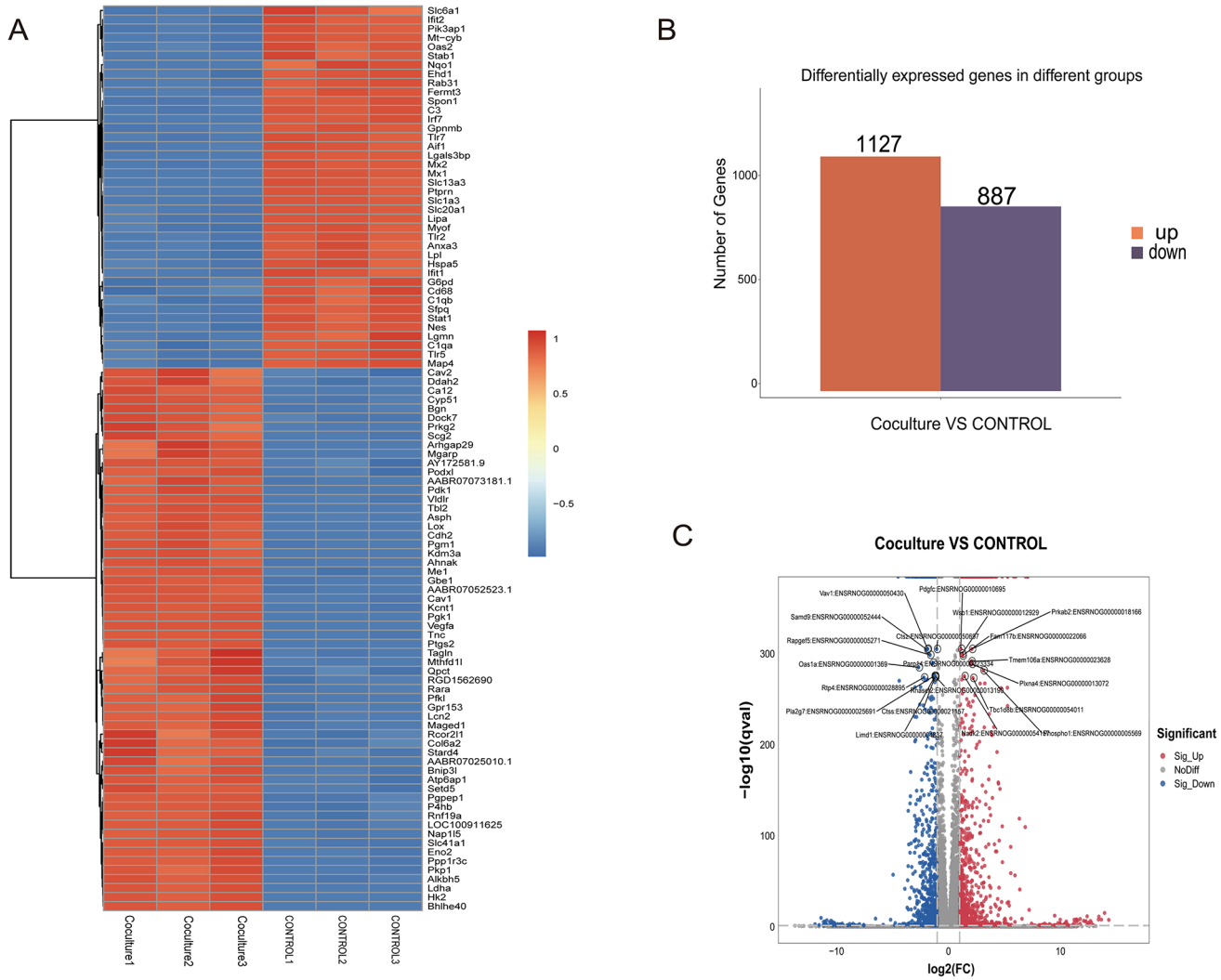

Fig. 1. Identification of differentially expressed genes (DEGs) in the control and coculture groups. (**A**) Heatmap of the differentially expressed genes. (**B**) Differentially expressed genes in the respective groups. (**C**) Volcano plot illustrating the identified differentially expressed genes.

Performing GO/KEGG enrichment analysis on the differentially expressed genes following coculture

A Gene Ontology (GO) functional enrichment analysis revealed that the differentially expressed genes (DEGs) were enriched in various biological processes (bp), particularly those related to signal transduction and immune response. In terms of molecular function, the DEGs were associated with protein binding, calcium binding, ATP binding, and metal ion binding. At the cellular component (cp) level, the DEGs were enriched in integral components of the membrane, cytoplasm, and the extracellular region. This analysis suggests that the co-culture model with hUCMSCs may influence NSCs through a variety of biological pathways and molecular interactions (Fig. 2A, B). KEGG pathway enrichment analysis[34] and corresponding diagrams indicated that the DEGs were predominantly enriched in several significant pathways. These include the PI3K-Akt signaling pathway, which is crucial for cell survival and growth; the neuroactive ligand-receptor signaling pathway, which is involved in neuronal communication; the cytokine-cytokine receptor interaction pathway, which plays a role in immune response regulation; the calcium signaling pathway, which is essential for intracellular signaling; the Rap1 signaling pathway, which is involved in cell migration and adhesion; and the HIF-1 signaling pathway, which is critical for cellular responses to hypoxia (The KEGG images were created with https://www.kegg.jp/kegg/kegg1.html, We have obtained the publication permission from Kanehisa Laboratory). The enrichment analysis suggests that the co-culture model with hUCMSCs may influence NSC behavior through a complex interplay of multiple signaling pathways (Fig. 2C, D). It was found that the genes included in the module are involved in processes such as regulating cell proliferation, cellular response to calcium ions, and PI3K-Akt signaling. Our goal was to identify the important proteins involved in these processes by building protein–protein interaction networks (PPI) using information from the STRING database on the differentially accumulated proteins in both the co-culture and control groups. The resulting PPI network included 119 nodes (proteins) and 508 edges (interactions) (Fig. 2E), providing a visual representation of the complex interplay among these proteins. From

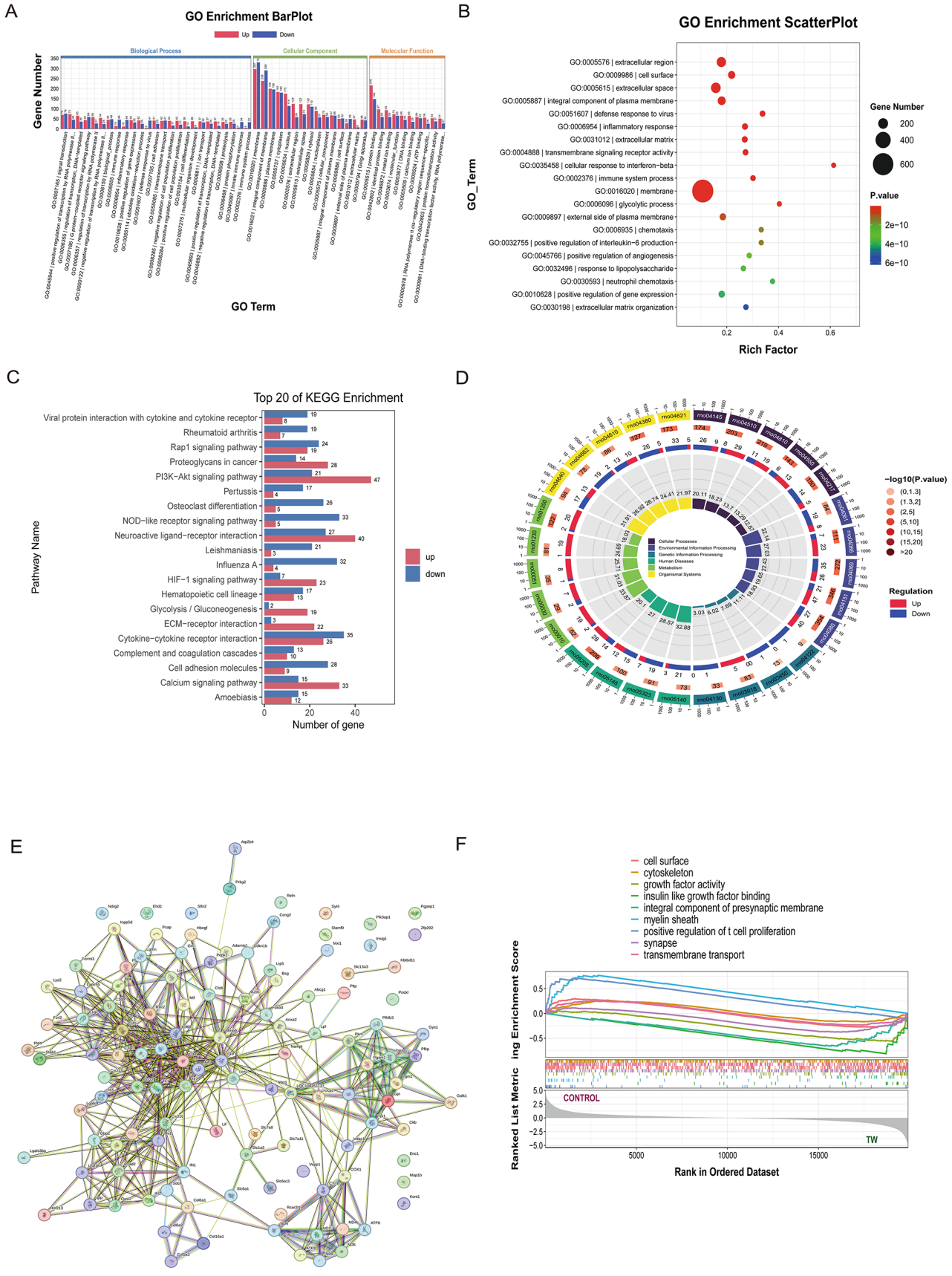

the top 10 most connected nodes in the PPI network, the following hub proteins were identified: Ptprc (CD45), Ltgb2 (Laminin gamma-2), CD68 (Cluster of Differentiation 68), Rac2 (Ras-related C3 botulinum toxin substrate 2), Csf1 (Colony Stimulating Factor 1), Cd4 (Cluster of Differentiation 4), Mmp9 (Matrix Metallopeptidase 9), and C3ar1 (Complement Component 3a Receptor 1). Among these, Ptprc had the highest degree of connectivity

◀**Fig. 2**. GO/KEGG enrichment analysis of differentially expressed genes after coculture. (**A**, **B**) Results of the Gene Ontology (GO) analysis with respect to biological processes. (**C**, **D**) Kyoto Encyclopedia of Genes and Genomes (KEGG) analysis. (**E**) Structure of the differentially expressed gene protein interaction network. (**F**) The GSEA (Gene Set Enrichment Analysis) enrichment analysis displays sorted genes on the horizontal axis and enriched scores on the vertical axis, with different colored curves representing distinct functions or pathways. Peaks on the upper left side of a curve suggest activation of the function or pathway in the control group, while peaks on the lower right side indicate activation in the coculture group.

within the network. Gene Set Enrichment Analysis (GSEA) enrichment plots revealed that pathways such as cell surface, cytoskeleton, growth factor, synapse, myelin sheath, and transmembrane transport were differentially enriched in the co-culture group compared to the control group (Fig. 2F), indicating that these pathways are likely to contribute to observed differences.

Detection of cell viability and NSCs proliferation efficiency in the co-culture model

Transwell chambers were employed to establish a co-culture model, wherein hUCMSCs were initially seeded in the lower chamber and NSCs were subsequently added to the upper chamber (which will be marked as hUCMSCs/NSCs, and vice versa). Cell viability was evaluated on days 1, 3, 7, and 14 of in vitro culture using the CCK-8 assay. The findings revealed that there were no statistically significant alterations in cell viability during the initial seven days of co-culture in the hUCMSCs/NSCs group (Fig. 3A). Nonetheless, by the fourteenth day, the CCK-8 results demonstrated a notable decrease in cell viability. Compared to the control group, where only the lower chamber seeded hUCMSCs, the coculture group (hUCMSCs/NSCs) showed lower cell activity (1.102 ± 0.02272 and 0.9376 ± 0.02503, respectively, $p = 0.007$). In a separate experiment, NSCs were initially seeded beneath the Transwell chamber, followed by the seeding of hUCMSCs above it (NSCs/hUCMSCs group) (Fig. 3B). Consistent with prior investigations, cell viability was evaluated at intervals of 1-, 3-, 7-, and 14-days during co-culture. Findings revealed that the relative viability of NSCs remained largely unaffected, potentially attributed to the inherently sluggish proliferation kinetics of NSCs. Notably, no evidence of contact inhibition was observed in contrast to the behavior exhibited by the hUCMSCs/NSCs group.

Following evaluation of the basal layer of hUCMSCs cells in the hUCMSCs/NSCs co-culture system utilizing Calcein/PI staining (Fig. 3C), our findings indicated no notable variance in cell viability between the co-culture and control groups on the DIV.7. Subsequently, within the NSCs/hUCMSCs co-culture system, EdU staining was employed to assess cell proliferation. The results revealed a significantly elevated proliferation rate in the co-culture group compared to the control group at both 3 days (DIV.3) and 7 days (DIV.7) of cultivation. However, on the first day (1.026 ± 0.02125 and 1.139 ± 0.02398, respectively, $p = 0.0056$) and third day (1.002 ± 0.01470 and 1.077 ± 0.02493, respectively, $p = 0.0260$) of culture, the cell activity in the co-culture group actually showed a certain degree of increase. This indicates that the presence of hUCMSCs in the co-culture environment may have a stimulating effect on the proliferation of NSCs (Fig. 3D). Among them, the proportion of EdU positive cells in vitro on the 3rd day was (24.84 ± 2.430 and $39.08 \pm 3.935\%$, respectively, $p = 0.0082$), and the proportion of EdU positive cells on the 7th day was (12.19 ± 1.198 and $18.62 \pm 1.661\%$, respectively, $p = 0.0033$).

Changes in the differentiation of neural stem cells (NSCs) in Co-culture model

This section of the research focused on examining the differentiation of neural stem cells (NSCs) within the co-culture system. Following a 7-day culture period in differentiation medium, a notable proportion of cells remained undifferentiated in both experimental groups, with a higher prevalence observed in the control group. Moreover, the co-culture group exhibited a significantly greater number of cells undergoing differentiation (Fig. 4A), as evidenced by markedly elevated levels of Tuj-1^+ (1.086 ± 0.09736 and 1.676 ± 0.1418, respectively, $p = 0.0020$) and $GFAP^+$ compared to the control group ($p = 0.1224$). In the co-culture group, we observed more pronounced neuronal cell bodies and axons, as well as astrocyte cell bodies (Fig. 4B).

The following observation concentrated on the intricate nature of differentiated neuronal cells as they contribute to the regeneration of neural networks at the site of injury. Subsequently, a detailed analysis of the complexity of these cells was conducted using Sholl analysis, a widely utilized quantitative technique for assessing dendritic arbor complexity. The Sholl profiles of cell tracings, as illustrated in Fig. 4C, revealed that neurons displayed increased complexity, branching, and elongation of neurites following co-culture compared to the control group. The co-culture group demonstrated enhanced average and maximum axon lengths, as measured by quantifying the number of intersections at 20 μm intervals extending up to 240 μm from the center of the cell body. Sholl analysis, which examines the pattern of neurite branching, also indicated a greater degree of neurite arborization in the co-culture group compared to the control group. These observations imply that the co-culture model promotes the differentiation of NSCs and contributes to the development of more complex and mature axonal structures in the resulting neuronal cells (Fig. 4D).

Stem cells can remain at the site of injury for an extended period

In this study, live cell staining was utilized to mark the transplanted cells, followed by in vivo imaging to monitor the fluorescence intensity at the injury site on days 1, 3, 7, and 14 post-transplantations. Our findings revealed that the fluorescence signal emanating from the transplanted cells was observable for a duration of up to 7 days, after which it progressively diminished. These results suggest that the transplanted cells have the capacity to persist at the injury site for a specific timeframe, enabling them to function within the challenging microenvironment of the injury site.

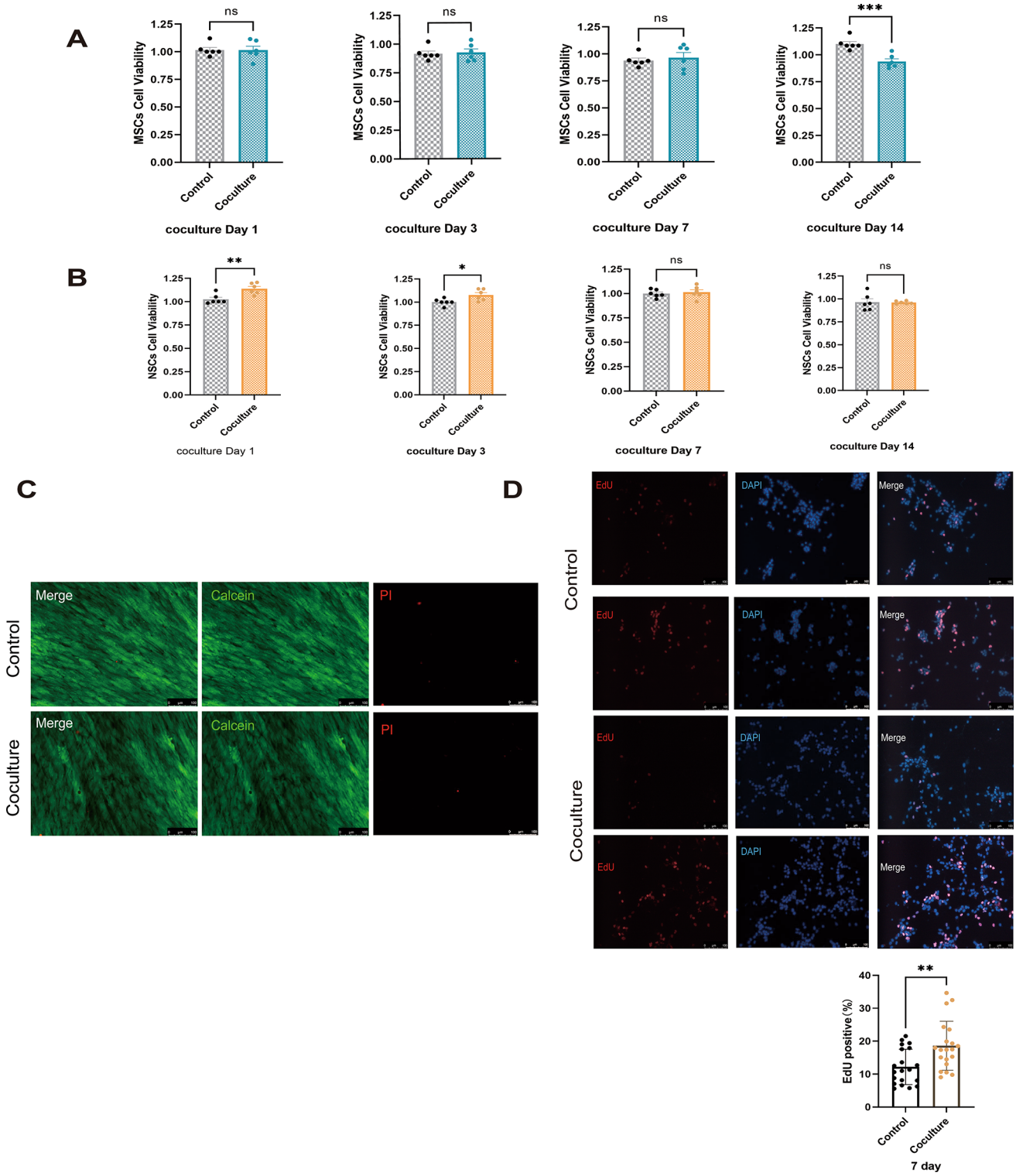

Fig. 3. In the co-culture model, the activity and proliferation of NSCs and hUCMSCs were detected. (Scale bar = 100 μm) (**A**, **B**) Cell viability was evaluated on days 1, 3, 7, and 14 of in vitro culture using the CCK-8 assay. Relative cell viability of the hUCMSCs/NSCs and NSCs/hUCMSCs cocultured model compared with control group (data shown as mean ± SEM, unpaired t-test, *P < 0.05, **P < 0.01, ***P < 0.001, n = 5). (**C**) Calcein/PI Live/dead cell dying was performed on hUCMSCs cells of the hUCMSCs/NSCs coculture Transwell model in day 3. (D) NSCs proliferation showed by EdU staining and quantitative assay in NSCs/hUCMSCs model in day 3 and day7. (data shown as mean ± SEM, unpaired t-test, *P < 0.05, **P < 0.01, ***P < 0.001, n = 8).

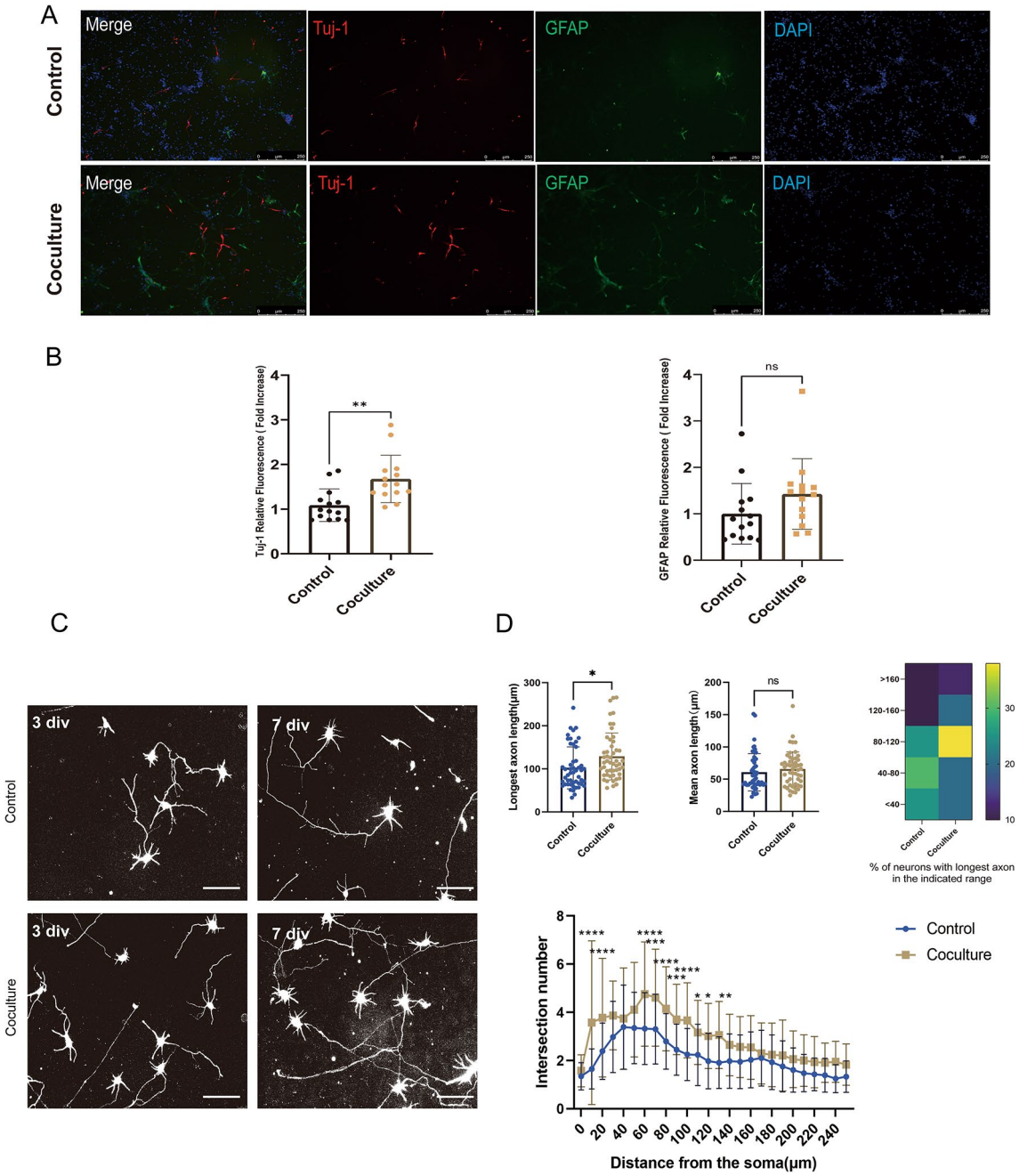

Fig. 4. In the NSCs/hUCMSCs co-culture model, analysis of NSCs differentiation and the complexity of axonal arborization in differentiated neurons was conducted. (**A**, **B**) Determination of NSCs differentiation towards neuronal and astrocytic lineages after 7 days in culture. (data shown as mean ± SEM, unpaired t-test, *P < 0.05, **P < 0.01, ***P < 0.001, n = 14) (Scale bar = 250 μm) (**C**) Quantitative measurement of the lengths and numbers of branches of outgrowing neurites obtained between the Control and Coculture group (data shown as mean ± SEM, unpaired t-test, *P < 0.05, **P < 0.01, ***P < 0.001, n = 40) (Scale bar = 50 μm) (**D**) Sholl profiles of the Control and Coculture groups. (data shown as mean ± SEM, one-way ANOVA with Tukey's post hoc test, *P < 0.05, **P < 0.01, ***P < 0.001, n = 40).

Meanwhile, we employed immunofluorescent staining with mouse anti-human specific nuclear antigen (HuNu) to examine the localization of human umbilical cord mesenchymal stem cells at the site of injury (Fig. 5A). Our investigation focused on the time points of 1-, 3-, 7-, and 14-days following implantation. The results depicted in the Fig. 5B indicate a notable presence of HuNu-labeled hUCMSCs on the initial day post-implantation, with a subsequent decline in labeled cell count on days 3 and 7. By day 14 following the injury, minimal HuNu-labeled signals were detected at the injury epicenter (Fig. 5C). These findings further support our in vivo imaging results, suggesting that while cell transplantation may initially endure at the injury locus, their functionality is ultimately impeded by the intricate microenvironment of the injury site.

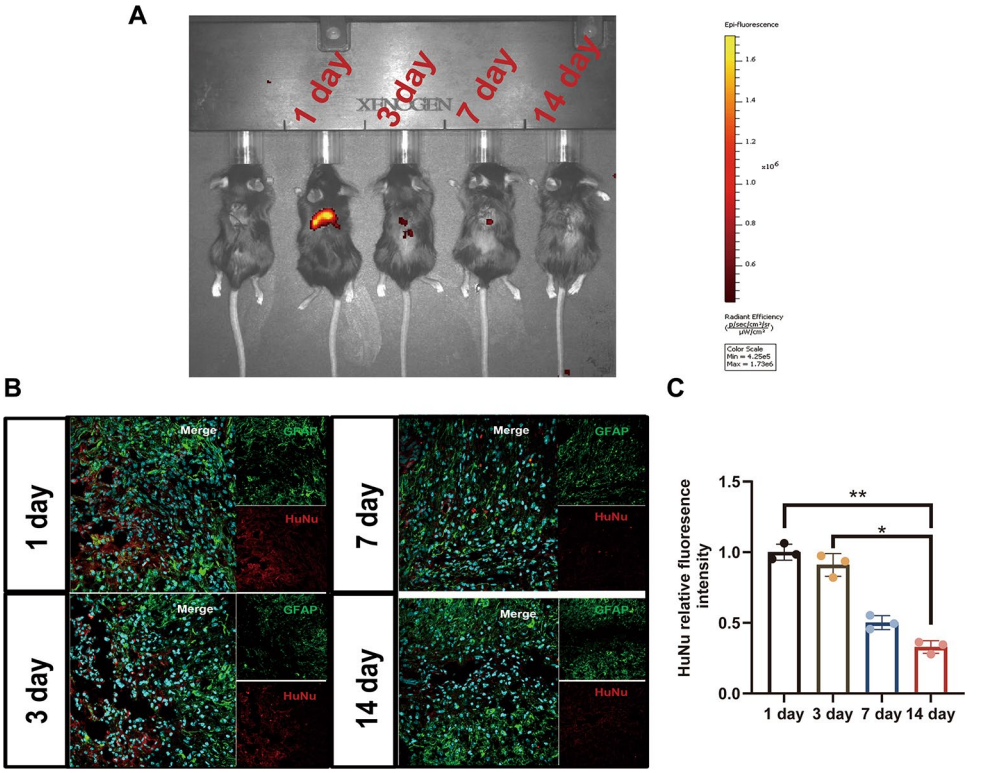

Fig. 5. The transplantation of hUCMSCs/NSCs cells can remain at the site of injury for an extended period. (**A**, **B**) Representative images of bioluminescence imaging depicting the injured spinal cord in situ at various time points (1 day, 3 days, 7 days, and 14 days) following spinal cord injury in the cell transplantation groups. (**B**, **C**) The variation in fluorescence intensity of HuNu at various time intervals within each experimental group serves as an indicator of the viability and survival rate of human umbilical cord mesenchymal stem cells. GFAP staining of astrocytes reveals the boundaries of the injury site. (data shown as mean ± SEM, one-way ANOVA with Tukey's post hoc test, Kruskal–Wallis test followed by the post hoc Mann–Whitney U test, $^{*}P < 0.05$, $^{**}P < 0.01$, n = 3) (Section = 10 μm, Scale bar = 50 μm).

The combined application of cell transplantation and epidural spinal cord electrical stimulation promotes better behavioral recovery in mice compared to cell transplantation or spinal cord stimulation alone

Figure 6A depicts the animal experiment procedure. After the spinal cord injury (SCI) model was established, all animals' Basso Mouse Scale (BMS) scores decreased to zero. An assessment of functional recovery following SCI was conducted by two trained observers at the following time points: 1 day prior to injury, 3, 7, 14, 21, 28, 35, 42, 49, and 56 days after injury. The BMS score is a widely used method to assess locomotor function in mice with SCI, and the observed changes in the score over time provide insights into the progression of functional recovery. Subsequently, one-week post-injury, the CT group underwent a dual-seed cell transplantation at a concentration of approximately 10^5/1μL (Fig. 6C). The EES group underwent the implantation of an epidural stimulation electrode (Fig. 6B), while the Combination group received the cell transplantation followed by the implantation of a spinal epidural electrode. Following treatment, functional recovery among the various cohorts was assessed on a weekly basis using the BMS locomotor rating scale. In our observations (Fig. 7A), mice in the injury group were still unable to bear weight on their hind limbs 56 days later, with their paws unable to touch the ground, and only limited ankle joint movement was noted. In the EES group, a small number of animals managed to achieve paw standing, while mice treated with hUCMSCs exhibited more frequent and sustained paw standings. However, there was still no coordinated gait observed. Meanwhile, the Combination treatment group showed improved coordination in their walking gait (Fig. 7B).

Simultaneously, the swimming test results exhibited analogous patterns to the BMS scores (Fig. 7C). Our observations indicated that the LSS score of the Injury group approached zero, signifying a lack of movement and alteration in their hind limbs, rendering them unable to contribute to swimming movements. Consequently, there was a notable dependence on the forelimbs for swimming. Furthermore, the subjects exhibited an inability to sustain stability in trunk instability. Conversely, both the EES and CT cohorts displayed enhancements in hind limb movement, with intermittent instances of 6–50% hind limb activity noted. Notably, the Combination group demonstrated superior swimming abilities, particularly in terms of improvements in trunk instability and body angle when compared to the other groups. This suggests that the combination therapy or treatment approach used in this group may be more effective in promoting functional recovery after spinal cord injury, as evidenced by the enhanced swimming performance (Fig. 7D).

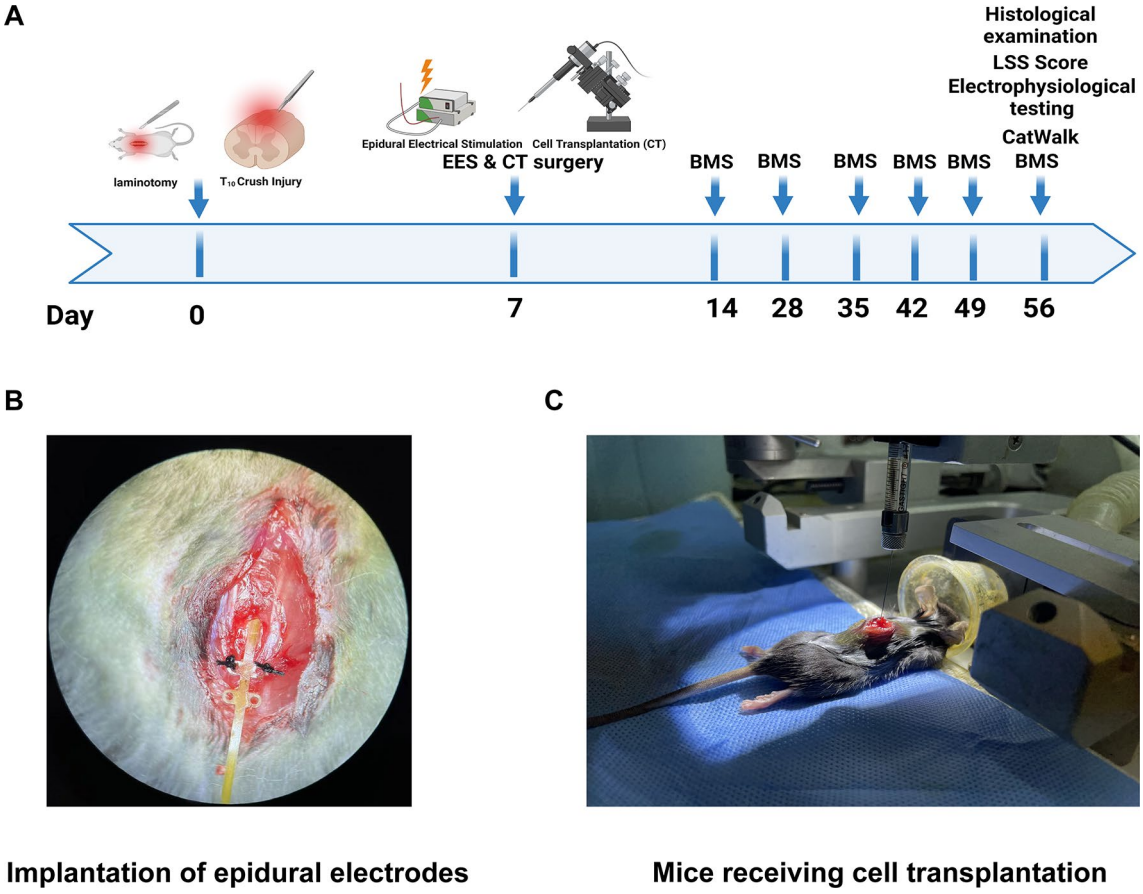

Fig. 6. In vivo experimental design, including cell transplantation and implantation of epidural electrodes. (**A**) Illustration depicting the experimental design for long-term experiments and motor function recovery evaluation. (The flowchart was created using BioRender.com, with the publication agreement number GX277Z3XGW). (**B**) Illustration of epidural electrode implantation under a stereoscopic microscope. After laminectomy, the epidural electrode is inserted in the rostral direction to ensure that the electrode contacts are positioned at the site of injury. Subsequently, the electrode's side ear is secured to the paravertebral muscle with surgical sutures. (**C**) Picture of in situ stem cell transplantation in SCI mice. As shown, under anesthesia, the stem cells are injected into the rostral, central, and caudal aspects of the injury site using a Hamilton micro syringe.

As mice's recovery progressed after 8 weeks post-injury, the CatWalk gait analysis system was used as an objective behavioral test method to measure locomotor function. This system provides a detailed analysis of gait parameters, such as stride length, stride width, and paw placement, which can be used to evaluate the extent of functional recovery after a spinal cord injury (Fig. 8). The results demonstrated significant improvements in multiple gait parameters including regularity index (%), step cycles, stride length, duty cycle, max contact area (cm^2), and print position phase in the hindlimbs. These findings suggest enhanced strength and coordination in the hindlimbs of mice with combination treatment.

Electrophysiological assays were conducted on mice to assess improvements in nerve conduction. Results from assessments performed 8 weeks post-injury revealed an increased MEP amplitude in the CT, EES, and Combination groups (Fig. 9C, D). The Combination therapy was determined to be the most effective approach for enhancing locomotor recovery in crush injury cases. This was evidenced by the recruitment of more gastrocnemius muscle fibers under the same stimulus intensity, leading to a larger MEP waveform and indicating a greater passage of corticospinal tract fibers through the injury site. Meanwhile, the Hematoxylin and Eosin (H&E) staining of the bladder revealed a greater thickness in the bladders of the spinal cord injury (SCI) mice that received combination therapy, indicating that the treatment group experienced significant improvement in urinary retention, as it suggests a better ability to store and empty urine, which is often compromised after SCI (Fig. 9A, B)[35].

Fibrotic scar ablation and the formation of astrocyte bridges were achieved in chronically injured mouse spinal cords after combinatorial treatment and cell transplantation

Reactive astrocytes form glial scars after central nervous system injury, exhibiting increased expression of glial fibrillary acidic protein (GFAP) and hypertrophy of cells. These reactive astrocytes surround the lesion site, creating a physical and biochemical barrier between the damaged area and the surrounding healthy tissue. The

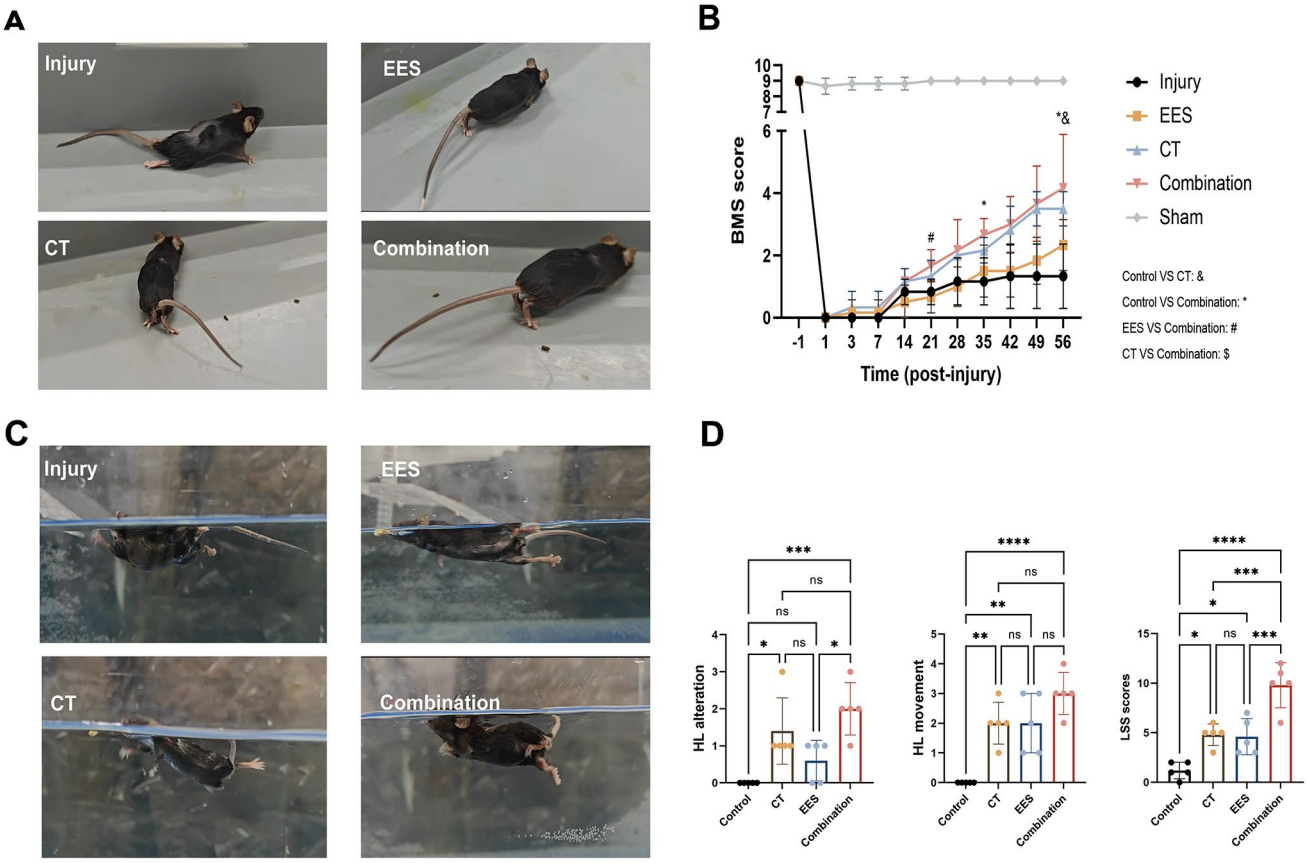

Fig. 7. Basso Mouse Scale for Locomotion and Louisville Swim Scale assessments in spinal cord-injured mice across different groups. (**A**) Photographs of mice undergoing BMS (Basso Mouse Scale) walking test at 56 days post-spinal cord injury in each group. (**B**) BMS score was observed by two trained observers at 1 day before, and 1, 3, 7, 14, 21, 28, 35, 42, 49 and 56 days after SCI. (**C**, **D**) Photographs of swimming test and comparison among three groups on LSS scores, including evaluation on hindlimb alteration and hindlimb movement. (data shown as mean ± SEM, Kruskal–Wallis test followed by the post hoc Mann–Whitney U test, *P < 0.05, ***P < 0.001, n = 5).

glial scar is thought to play a role in limiting the spread of damage and providing a scaffold for axonal regrowth, although it can also impede neural regeneration and functional recovery[36,37].

Fibrotic scar formation typically begins within days after a spinal cord injury and progresses over time. Research has indicated that the peak number of fibroblasts occurs at 7 days post-injury, primarily due to the inherent proliferation of fibroblasts within the spinal cord[38]. Specifically, within days after the injury, the inflammatory response at the injury site guides the migration and activation of immune cells and fibroblasts, fibroblasts begin to actively produce collagen and other extracellular matrix components, leading to the formation of the fibrotic scar. The fibrotic scar's composition features fibroblasts, microglia, and interstitial cells at its core [39]. Hence, immunofluorescence staining was employed to assess the impact of cell transplantation and EES on the fibrotic scar at 56 days post-injury (dpi), specifically targeting the expression of PDGFR-β and GFAP. The findings revealed a notable reduction in the density of PDGFRβ + cells in the combination group compared to the other groups at 56 dpi (Fig. 10A). Moreover, the fibrotic scar area was found to be smaller in the stem cell transplantation group as opposed to the EES group, suggesting that stem cell transplantation primarily influences the formation of fibrotic scars. Emerging evidence indicates that astrocytes possess a heightened potential to enhance axon regeneration within the damaged central nervous system, extending beyond conventional understanding, in proximity to and distant from the site of injury. The mechanisms through which astrocytes facilitate axon elongation and foster growth encompass the release of neurotrophic factors, modification of the extracellular matrix, clearance of cellular waste, and provision of metabolic sustenance[40]. In our study, it was observed that the combined treatment group, which underwent cell transplantation, exhibited a notably larger $GFAP^+$ bridging area in comparison to both the single cell transplantation group and the EES group (Fig. 10B,C). This finding underscores the efficacy of cell transplantation therapy in mitigating fibrotic scar formation at the site of injury and facilitating the extension of the $GFAP^+$ bridge, thereby fostering axon regeneration within the lesion.

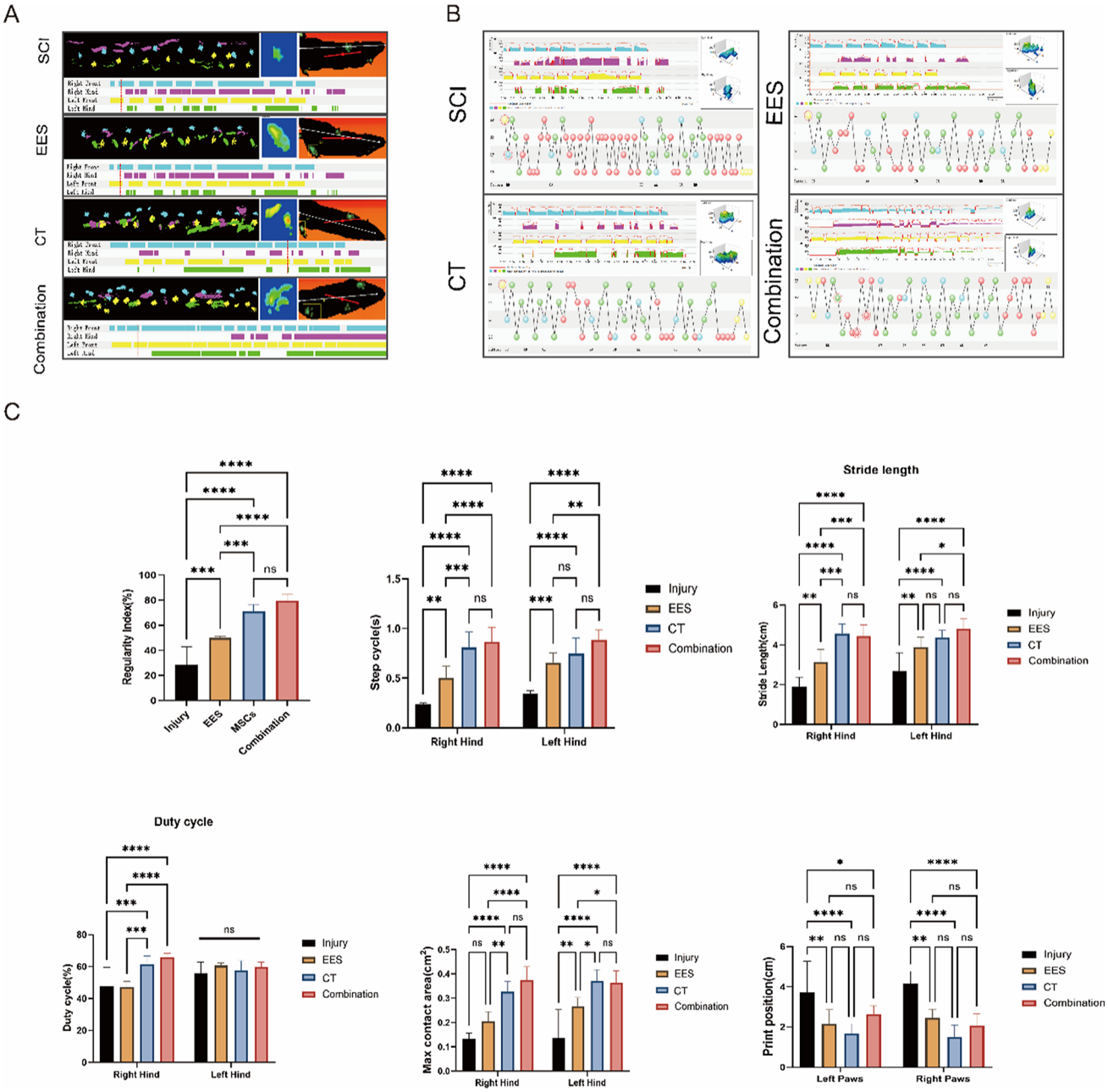

Fig. 8. CatWalk gait analysis for each group and intergroup comparisons. (**A**) Representative images of footprint tracks with color coding: Left Front (yellow), left hind (green); Right Front (blue), right hind limb (purple). (**B**) Representative images of 2D Footprint Intensities and Footfall Patterns. (**C**) Statistical analysis of six commonly used CatWalk parameters: Regularity Index (%), Step Cycles (s), Stride Length (cm), Duty Cycle (%), Maximum Contact Area (cm^2), Print Position (cm). The results for the Regularity Index (%) were derived from the analysis of all four limbs, while the others were obtained from the analysis of the hindlimbs. (data shown as mean ± SEM, one-way ANOVA with Tukey's post hoc test, $^*P < 0.05$, $^{**}P < 0.01$, $^{***}P < 0.001$, n = 5).

The combinatorial approach and cell transplantation effectively shifted the polarization of macrophages/microglia towards the M2 phenotype in the context of in vivo treatment

Prior research has demonstrated that the in situ injection transplantation of hUCMSCs[41] or NSCs[42] can successfully attenuate inflammation levels during the acute stage of spinal cord injury and decrease neuronal apoptosis at the site of injury. Consequently, our study focused on investigating the polarization direction of the infiltrated macrophages/microglia. A combination therapy and cell transplantation effectively influenced macrophage/microglial polarization toward the M2 phenotype in vivo. In the investigation of macrophage polarization dynamics following spinal cord injury (SCI), Induced nitric oxide synthase (iNOS) and arginase 1 (Arg1) levels were quantified as markers of M1 and M2 inflammation, respectively. The results showed a greater number of cells expressing both iNOS and CD68 in the injury group compared to the other groups,

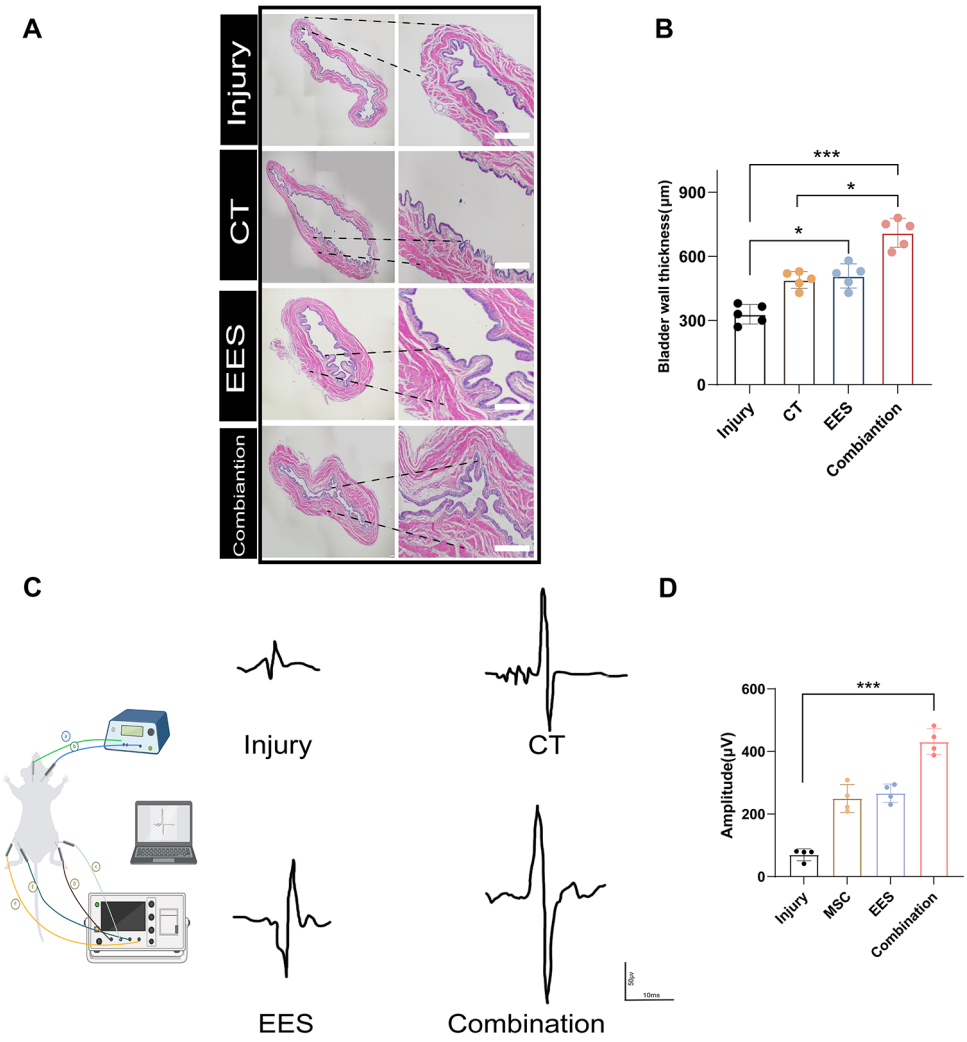

Fig. 9. Electrophysiological assessments of spinal conduction recovery, as well as the assessment of bladder micturition function. (**A**) The H&E staining of the bladder showed the thickness comparison in the SCI mice. (Section:4 μm, Scale bar = 250 μm) (**B**) Quantification of the bladder wall thickness. (data shown as mean ± SEM, Kruskal–Wallis test followed by the post hoc Mann–Whitney U test, *P < 0.05, ***P < 0.001, n = 5) (**C**) Representative MEP waveform of nerve electrophysiology examination of mice in each group at 56 days post-SCI. (**D**) Quantification of the motor evoked potentials (MEP) in each group of spinal cord-injured mice at the experimental endpoint 56 days. (data shown as mean ± SEM, one-way ANOVA with Tukey's post hoc test, *P < 0.05, **P < 0.01, ***P < 0.001, n = 5).

indicating a higher presence of the pro-inflammatory M1 phenotype at the injury site. Conversely, the presence of this M1-associated phenotype was reduced through the implementation of cell transplantation (see Fig. 11A, B). The upregulation of Arg1 + CD68 + cells, which are indicative of the M2 phenotype, was observed in the groups that underwent cell transplantation intervention (Fig. 11C, D). Stem cell transplantation modulates the inflammatory microenvironment in the early stages of injury, the findings suggest.

Discussion

A stem cell transplant is one of the most commonly used experimental treatments for spinal cord injuries[43]. In clinical trials, various types of stem cells have been examined, including neural progenitor cells [16], embryonic cells[44], hematopoietic cells[45], bone marrow mesenchymal stem cells[46], adipose-derived mesenchymal stem cells[47] and umbilical cord stem cells[48]. Most of these trials have yielded promising results. However, it is crucial to recognize that the therapeutic benefits of stem cells have limitations. Presently, the majority of clinical investigations pertaining to stem cell therapy are centered on individuals in the subacute or chronic phases of injury, with minimal attention given to those in the acute phase. However, many unresolved inquiries persist, encompassing the determination of the most effective dosage and timing, the assessment of cell survival and persistence at the injury site, the clarification of differentiation and integration processes, the examination of interactions with the immune system, the establishment of standardized protocols, the identification of appropriate candidates, and the evaluation of efficacy in combination therapies, the evaluation of potential risks

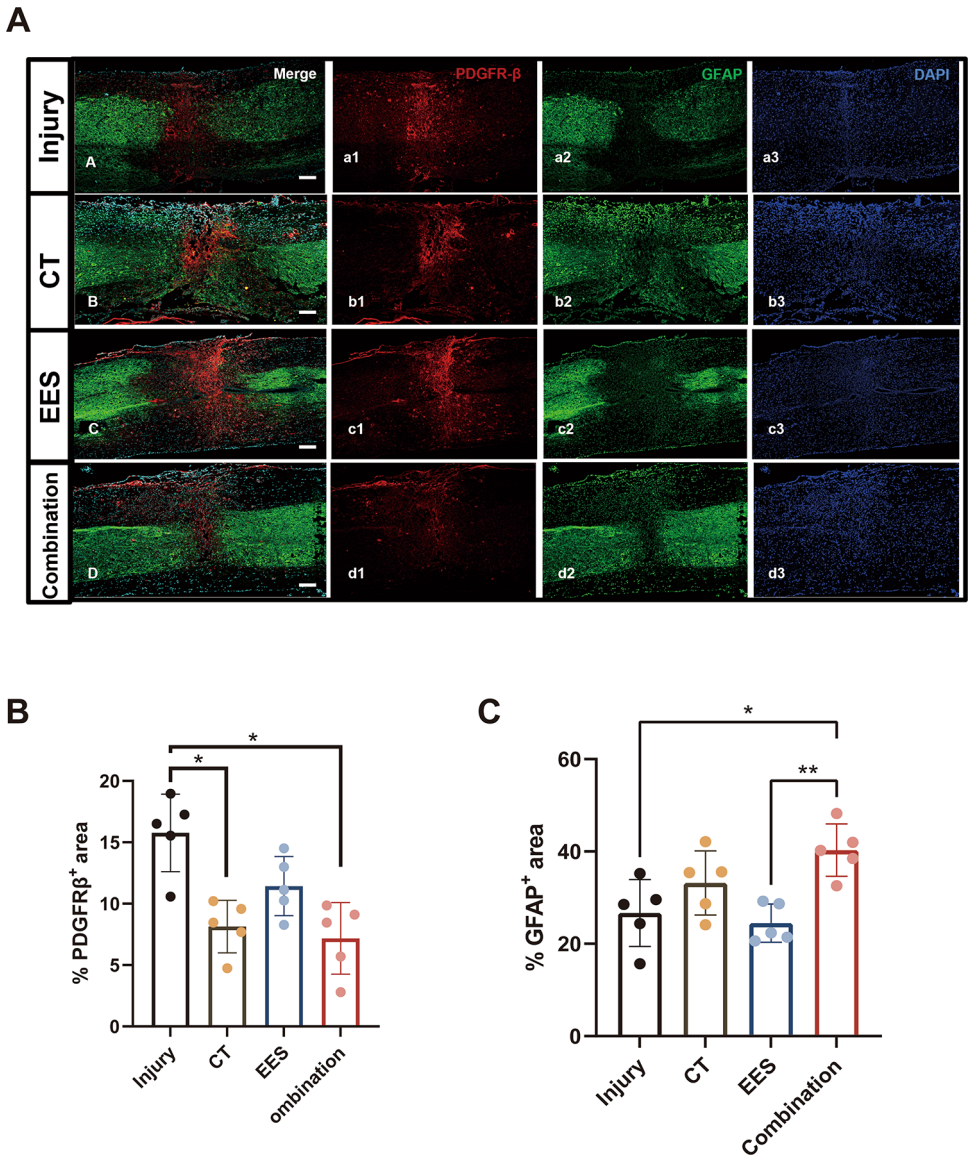

Fig. 10. A decrease in fibrotic scar formation and formation of astrocytic bridges was noted in both the cell transplantation group and the combined treatment group. (**A**) Spatiotemporal distribution of PDGFR-β following spinal cord injury. Immunofluorescence staining of PDGFRβ (red), GFAP (green) and nuclei (blue) in sagittal sections at 56 days post-injury. (Section = 10 μm, Scale bar = 100 μm) (**B**) Quantification of the PDGFRβ$^+$ and GFAP$^+$ in each group of spinal cord-injured mice at the experimental endpoint 56 days. (data shown as mean ± SEM, Kruskal–Wallis test followed by the post hoc Mann–Whitney U test,, *$P < 0.05$, **$P < 0.01$, $n = 5$).

such as tumorigenicity and immunogenicity[49]. Especially in studies involving the co-transplantation of various types of seed stem cells, it is crucial to consider the cellular interactions between the transplanted seed cells[50].

On the other hand, spinal cord stimulation has been extensively utilized in clinical settings to facilitate the rehabilitation of patients in the chronic phases of injury[22]. Specifically, it offers notable benefits in managing post-spinal cord pathological pain[51], and advancements in spinal cord epidural stimulation (SCS) have been notable in recent years. Researchers have enhanced the precision of stimulation electrode placement and refined the targeting of selective activation of functional motor neurons[52]. Rowald et al. [53]and Herrity et al.[54] integrated human spinal imaging data to create a repository of three-dimensional models, and utilized computer simulation tools to analyze the distribution of electric fields during spinal cord stimulation (SCS) in order to inform the development of epidural electrodes. Rowald et al.[53] employed mechanical vibration on tendons to amplify muscle spindle afferent signals, thereby augmenting patient proprioceptive feedback, and subsequently monitored alterations in spinal cord oxygen levels. Verification was performed at the ankle, knee, and hip joint levels to observe the correlation between the internal oxygen levels of the spinal cord and the afferent impulses. The results demonstrated that the precise application of electrical stimulation to selectively enhance

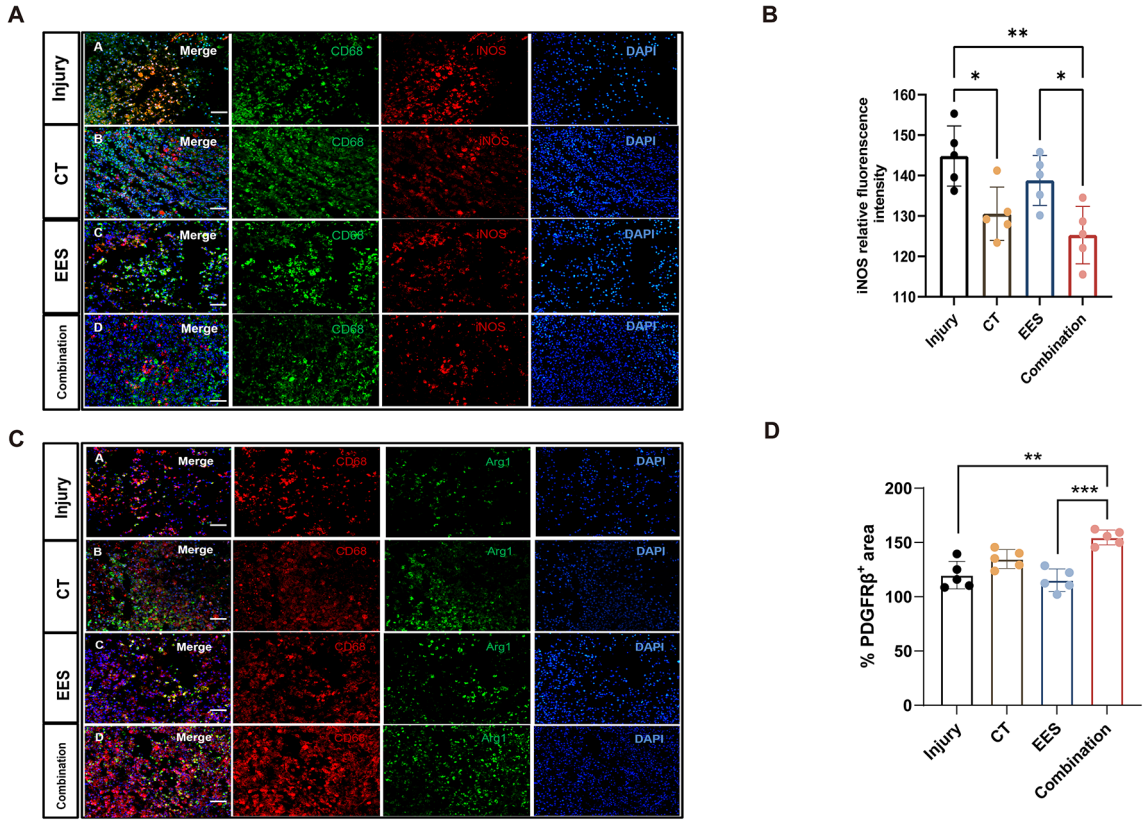

Fig. 11. Combined treatment effectively improved the recovery of spinal cord injury (SCI) mice through the regulation of microglial polarization and inhibition of the inflammatory response. (**A**) Immunofluorescence staining of iNOS and CD68 in spinal cord Sects. 14 days after spinal cord injury. (Section = 10 μm, Scale bar = 50 μm) (**B**) The image analysis findings are displayed as the average relative fluorescence intensity of iNOS (n = 5). (**C**) Immunofluorescence staining of Arg1 and CD68 in spinal cord Sects. 3 days after spinal cord injury. (**D**) The image analysis findings are displayed as the average relative fluorescence intensity of Arg1 (data presented as mean ± SEM, Kruskal–Wallis test followed by the post hoc Mann–Whitney U test, *P < 0.05, **P < 0.01, ***P < 0.001, n = 5).

the excitability of the spinal cord's motor network shows potential for aiding in the recovery of motor function in patients with spinal cord injuries.

However, the current challenge in spinal cord injury treatment is the lack of a single strategy that can effectively provide comprehensive and sequential therapy throughout the various stages of the injury[55]. Individual treatment modalities often have restricted therapeutic scopes and encounter difficulties in implementing tailored interventions for the distinct characteristics of each stage of spinal cord injury[56]. Thus, the development of combination therapies for this debilitating chronic condition holds promise in offering valuable insights for the clinical management of spinal cord injuries. Numerous combined therapy approaches have shown advancements in the field, including the combination of cellular transplants with neurotrophins, the integration of cellular transplants with anti-inhibitory therapies, the amalgamation of anti-inhibitory therapies with neurotrophins, and the incorporation of various therapies with rehabilitation[55]. In a recent study led by Wang et al. [57], the combined administration of hUCMSCs and ultrashort wave therapy was found to effectively reduce neuroinflammation following spinal cord injury in rats. And this therapeutic effect was mediated through the NUR77/NF-κB pathway. This treatment also resulted in decreased activation of M1-type microglia and A1-type astrocytes, ultimately leading to functional restoration. Fuhrmann et al. conducted a study that involved delivering human induced pluripotent stem cell-derived oligodendrocyte progenitor cells (iPSC-OPCs) using platelet-derived growth factor (PDGF) within a hyaluronan methylcellulose hydrogel. Although the use of biomaterials improved the survival of the transplanted cells, the study did not observe significant improvements in functional recovery in a rat model of T2 spinal cord injury[58]. In a study conducted by the Elliott Donaghue's team, it was observed that the simultaneous administration of the anti-inhibitory microenvironment antagonist Anti-Nogo-A and the neurotrophic factor NT-3 resulted in enhanced behavioral recovery compared to single treatments, which only improved partial histological indicators[59]. These findings underscore the significance of integrating multiple treatment strategies to achieve optimal outcomes, especially when aiming to promote behavioral restoration in patients with spinal cord injuries.

The present study represents, to the best of our knowledge, the first exploration of a treatment strategy that combines the transplantation of hUCMSCs and NSCs with EES. Our research aims to combine these two widely

utilized tissue engineering seed cells with SCS, a commonly employed rehabilitation treatment, in order to offer valuable insights for clinical application.

In the present study, we examined the interplay between two distinct seed stem cell types within an in vitro Transwell co-culture model. Our findings indicate that the cell viability of both groups remained relatively stable throughout the 14-day culture period. Interestingly, the proliferation rate of neural stem cells (NSCs) was modestly increased when positioned in the lower layer of the co-culture system. Furthermore, mRNA sequencing and bioinformatics analysis were conducted on the NSCs, uncovering variations in enrichment in various pathways such as regulation of cell proliferation, cellular response to calcium ions, and the PI3K-Akt signaling pathway, as well as cell surface, cytoskeleton, growth factor, synapse, myelin sheath, and transmembrane transport. Following this, the efficacy of neuronal and astrocytic lineage differentiation of NSCs was investigated. The findings indicated a heightened neuronal differentiation in the co-culture group. Utilizing Sholl analysis for evaluating the morphological intricacy of neurons, our study revealed that neurons cultured under co-culture conditions displayed heightened complexity and maturity in their neuronal morphologies.

Following this, the effectiveness of the combined treatment was confirmed in a mouse spinal cord crush injury model. At 1-week post-injury, in situ cell transplantation and epidural electrode implantation were performed. The survival rate of hUCMSCs transplanted in situ was evaluated through live imaging and HuNu immunofluorescence staining. The results indicated a gradual decrease in cell survival efficiency post-transplantation, leading to undetectable levels by day 14 post-transplantation. Subsequently, behavioral assessments were performed utilizing BMS, LSS scores, and the CatWalk gait analysis system. The behavioral outcomes demonstrated that the combined treatment group exhibited better recovery compared to the groups receiving individual treatments. Since behavioral recovery is the gold standard for assessing spinal cord injury outcomes, our results validate that the combined treatment strategy can more effectively achieve sequential therapy during both the acute and chronic phases of injury. Subsequently, attention was directed towards the injury site, where assessments were made on scar formation, astrocytic bridge area, acute phase microglia/macrophage polarization direction, and bladder wall thickness. It was observed that cell transplantation with in situ injection and the combined treatment group effectively regulated the acute phase inflammatory microenvironment and fibrous scar formation at the injury site. This study demonstrated the positive effects of epidural electrical stimulation (EES) on functional recovery, which may be related to promoting neural regeneration at the site of injury. Additionally, it may be associated with enhanced activity of the central pattern generator (CPG) in the lumbar spinal cord. In our experiment, the electrical stimulation protocol employed was relatively simple, compared to existing schemes such as high-frequency electrical stimulation or those assisted by artificial intelligence. Consequently, the full advantages of spinal cord stimulation may not have been fully realized in our study.

In the future, the treatment of spinal cord injuries will necessitate a collaborative and sequential approach incorporating various interventions. Even considerations for the psychological well-being of patients must also be integrated[60]. Our research proposes an integrated, sequential treatment strategy derived from established treatment protocols, presenting a novel framework for future spinal cord injury repair.

Conclusion

In our study, we proposed for the first time a combined transplantation strategy of human umbilical cord mesenchymal stem cells and neural stem cells combined with epidural electrical stimulation. We initially demonstrated the synergistic effect of co-culture of the two cell types in vitro. Subsequently, in a long-term trial with mice under crush injury, we found that the combined treatment strategy significantly improved behavioral recovery compared to the monotherapy. Furthermore, the detection of cells transplanted in situ during the acute phase revealed that cell transplantation could reduce inflammation at the early stage of injury and decrease fibrotic scar formation in the later stage. The intervention treatment methods in this study, such as stem cell therapy and spinal cord stimulation, have corresponding clinical trial plans that are currently ongoing, which are expected to provide beneficial guidance for future treatments. Our experiments provide an effective theoretical support for the long-term sequential treatment of patients after spinal cord injury.

Data availability

The data that support the findings of this study are available from the corresponding author upon reasonable request.The sequencing data have been uploaded onto the Gene Expression Omnibus with the accession number: BioProject PRJNA1128795.

Received: 16 July 2024; Accepted: 8 October 2024
Published online: 30 October 2024

References

1. Fan, B., Wei, Z. & Feng, S. Progression in translational research on spinal cord injury based on microenvironment imbalance. *Bone Res.* **10**(1), 35 (2022).
2. Liu, Y. et al. Spinal cord injury: global burden from 1990 to 2019 and projections up to 2030 using Bayesian age-period-cohort analysis. *Front Neurol.* **14**, 1304153 (2023).
3. Global, regional, and national burden of traumatic brain injury and spinal cord injury, 1990–2016: A systematic analysis for the Global Burden of Disease Study 2016. Lancet Neurol, 2019. **18**(1), 56–87.
4. Fan, B. et al. Microenvironment imbalance of spinal cord injury. *Cell Transpl.* **27**(6), 853–866 (2018).
5. Karsy, M. & Hawryluk, G. Modern medical management of spinal cord injury. *Curr. Neurol. Neurosci. Rep.* **19**(9), 65 (2019).
6. Lee, B. J. & Jeong, J. H. Early decompression in acute spinal cord injury: Review and update. *J. Korean Neurosurg. Soc.* **66**(1), 6–11 (2023).

7. Lee, B. J. & Jeong, J. H. Review: Steroid use in patients with acute spinal cord injury and guideline update. *Korean J. Neurotrauma* **18**(1), 22–30 (2022).
8. Duan, R. et al. Clinical benefit of rehabilitation training in spinal cord injury: A systematic review and meta-analysis. *Spine (Phila Pa 1976)* **46**(6), e398–e410 (2021).
9. Dasari, V. R., Veeravalli, K. K. & Dinh, D. H. Mesenchymal stem cells in the treatment of spinal cord injuries: A review. *World J. Stem Cells* **6**(2), 120–133 (2014).
10. Bao, C. S. et al. Transplantation of Human umbilical cord mesenchymal stem cells promotes functional recovery after spinal cord injury by blocking the expression of IL-7. *Eur. Rev. Med. Pharmacol. Sci.* **22**(19), 6436–6447 (2018).
11. Xiao, X. et al. Human umbilical cord mesenchymal stem cells-derived extracellular vesicles facilitate the repair of spinal cord injury via the miR-29b-3p/PTEN/Akt/mTOR axis. *Cell Death Discov.* **7**(1), 212 (2021).
12. Deng, W. S. et al. Collagen scaffold combined with human umbilical cord-mesenchymal stem cells transplantation for acute complete spinal cord injury. *Neural Regen. Res.* **15**(9), 1686–1700 (2020).
13. Kong, D. et al. hiPSC-derived NSCs effectively promote the functional recovery of acute spinal cord injury in mice. *Stem Cell Res. Therapy* **12**(1), 172 (2021).
14. Lee, S. et al. Advances in neural stem cell therapy for spinal cord injury: Safety, efficacy, and future perspectives. *Neurospine* **19**(4), 946–960 (2022).
15. Shang, Z., et al., What is the optimal timing of transplantation of neural stem cells in spinal cord injury? A systematic review and network meta-analysis based on animal studies. Front. Immunol. **13** (2022).
16. Levi, A. D. et al. Clinical outcomes from a multi-center study of human neural stem cell transplantation in chronic cervical spinal cord injury. *J. Neurotrauma* **36**(6), 891–902 (2019).
17. Ghobrial, G. M. et al. Human neural stem cell transplantation in chronic cervical spinal cord injury: Functional outcomes at 12 months in a phase ii clinical trial. *Neurosurgery* **64**(CN_suppl_1), 87–91 (2017).
18. Mukhametova, E. et al. Consecutive transcutaneous and epidural spinal cord neuromodulation to modify clinical complete paralysis—the proof of concept. *Mayo Clin. Proc. Innov. Qual. Outcomes* **8**(1), 1–16 (2024).
19. Melzack, R. & Wall, P. D. Pain mechanisms: A new theory. *Science* **150**(3699), 971–979 (1965).
20. Pinter, M. M., Gerstenbrand, F. & Dimitrijevic, M. R. Epidural electrical stimulation of posterior structures of the human lumbosacral cord: 3. Control of spasticity. *Spinal Cord.* **38**(9), 524–531 (2000).
21. Joshi, K. et al. Spinal cord epidural stimulation improves lower spine sitting posture following severe cervical spinal cord injury. *Bioengineering* **10**(9), 1065 (2023).
22. Zhou, M. et al. Comparison of clinical outcomes associated with spinal cord stimulation (SCS) or conventional medical management (CMM) for chronic pain: A systematic review and meta-analysis. *Eur. Spine J.* **32**(6), 2029–2041 (2023).
23. Squair, J. W. et al. Neuroprosthetic baroreflex controls haemodynamics after spinal cord injury. *Nature* **590**(7845), 308–314 (2021).
24. Hachmann, J. T. et al. Electrical neuromodulation of the respiratory system after spinal cord injury. *Mayo Clin. Proc.* **92**(9), 1401–1414 (2017).
25. Lee, Y. J. et al. Effect of early sacral neuromodulation on bladder function in a rat model of incomplete spinal cord injury due to focal contusion. *Neuromodulation* **22**(6), 697–702 (2019).
26. Reynolds, B. A. & Weiss, S. Generation of neurons and astrocytes from isolated cells of the adult mammalian central nervous system. *Science* **255**(5052), 1707–1710 (1992).
27. Reynolds, B. A. & Weiss, S. Clonal and population analyses demonstrate that an EGF-responsive mammalian embryonic CNS precursor is a stem cell. *Dev. Biol.* **175**(1), 1–13 (1996).
28. Weinger, J. G. et al. Intraspinal transplantation of mouse and human neural precursor cells. *Curr. Protoc. Stem Cell Biol.* **26**, 2d.16.1-2d.16.16 (2013).
29. Dahlen, J. E. et al. Morphological analysis of activity-reduced adult-born neurons in the mouse olfactory bulb. *Front Neurosci.* **5**, 66 (2011).
30. Basso, D. M. et al. Basso mouse scale for locomotion detects differences in recovery after spinal cord injury in five common mouse strains. *J. Neurotrauma* **23**(5), 635–659 (2006).
31. Xing, C. et al. Correlation analysis between magnetic resonance imaging-based anatomical assessment and behavioral outcome in a rat contusion model of chronic thoracic spinal cord injury. *Front Neurosci.* **16**, 838786 (2022).
32. Liu, S. et al. Coordination function index: A novel indicator for assessing hindlimb locomotor recovery in spinal cord injury rats based on catwalk gait parameters. *Behav. Brain Res.* **459**, 114765 (2024).
33. Zhou, M. et al. Contact separation triboelectric nanogenerator based neural interfacing for effective sciatic nerve restoration. *Adv. Funct. Mater.* **32**(22), 2200269 (2022).
34. Kanehisa, M. et al. KEGG for taxonomy-based analysis of pathways and genomes. *Nucleic Acids Res.* **51**(D1), D587-d592 (2023).
35. Fouad, K. et al. Transplantation and repair: Combined cell implantation and chondroitinase delivery prevents deterioration of bladder function in rats with complete spinal cord injury. *Spinal Cord.* **47**, 727–732 (2009).
36. Wanner, I. B. et al. Glial scar borders are formed by newly proliferated, elongated astrocytes that interact to corral inflammatory and fibrotic cells via STAT3-dependent mechanisms after spinal cord injury. *J. Neurosci.* **33**(31), 12870–12886 (2013).
37. Hara, M. et al. Interaction of reactive astrocytes with type I collagen induces astrocytic scar formation through the integrin-N-cadherin pathway after spinal cord injury. *Nat. Med.* **23**(7), 818–828 (2017).
38. Li, Z. et al. Fibrotic scar after spinal cord injury: Crosstalk with other cells, cellular origin, function, and mechanism. *Front Cell Neurosci.* **15**, 720938 (2021).
39. Dias, D. O. & Göritz, C. Fibrotic scarring following lesions to the central nervous system. *Matrix Biol.* **68–69**, 561–570 (2018).
40. Hemati-Gourabi, M. et al. Capacity of astrocytes to promote axon growth in the injured mammalian central nervous system. *Front Neurosci.* **16**, 955598 (2022).
41. Zhu, X. et al. Neuroprotective effects of human umbilical cord-derived mesenchymal stem cells from different donors on spinal cord injury in mice. *Front Cell Neurosci.* **15**, 768711 (2021).
42. Guo, W. et al. The roles and applications of neural stem cells in spinal cord injury repair. *Front Bioeng. Biotechnol.* **10**, 966866 (2022).
43. Montoto-Meijide, R., et al., Mesenchymal stem cell therapy in traumatic spinal cord injury: A systematic review. *Int. J. Mol. Sci.* **24**(14) (2023).
44. Shroff, G. & Gupta, R. Human embryonic stem cells in the treatment of patients with spinal cord injury. *Ann. Neurosci.* **22**(4), 208–216 (2015).
45. Deda, H. et al. Treatment of chronic spinal cord injured patients with autologous bone marrow-derived hematopoietic stem cell transplantation: 1-year follow-up. *Cytotherapy* **10**(6), 565–574 (2008).
46. Kim, G. U., et al., Therapeutic potential of mesenchymal stem cells (MSCs) and MSC-derived extracellular vesicles for the treatment of spinal cord injury. *Int. J. Mol. Sci.* **22**(24) (2021).
47. Hur, J. W. et al. Intrathecal transplantation of autologous adipose-derived mesenchymal stem cells for treating spinal cord injury: A human trial. *J. Spinal Cord. Med.* **39**(6), 655–664 (2016).
48. Yang, Y. et al. Human umbilical cord mesenchymal stem cells to treat spinal cord injury in the early chronic phase: study protocol for a prospective, multicenter, randomized, placebo-controlled, single-blinded clinical trial. *Neural Regen Res.* **15**(8), 1532–1538 (2020).
49. Assinck, P. et al. Cell transplantation therapy for spinal cord injury. *Nature Neurosci.* **20**(5), 637–647 (2017).

50. Jiao, Q., et al., Cell-cell connection enhances proliferation and neuronal differentiation of rat embryonic neural stem/progenitor cells. Front. Cell. Neurosci. **11** (2017).
51. Traeger, A. C. et al. Spinal cord stimulation for low back pain. *Cochrane Database Syst. Rev.* **3**(3), Cd014789 (2023).
52. Cuellar, C. et al. Selective activation of the spinal cord with epidural electrical stimulation. *Brain Sci.* **14**(7), 650 (2024).
53. Rowald, A. et al. Activity-dependent spinal cord neuromodulation rapidly restores trunk and leg motor functions after complete paralysis. *Nat. Med.* **28**(2), 260–271 (2022).
54. Herrity, A. N. et al. Targeting bladder function with network-specific epidural stimulation after chronic spinal cord injury. *Sci. Rep.* **12**(1), 11179 (2022).
55. Griffin, J. M. & Bradke, F. Therapeutic repair for spinal cord injury: combinatory approaches to address a multifaceted problem. *EMBO Mol. Med.* **12**(3), e11505 (2020).
56. McIntyre, A. et al. A scoping review of self-management interventions following spinal cord injury. *Top. Spinal Cord. Inj. Rehabil.* **26**(1), 36–63 (2020).
57. Wang, S. et al. HUCMSCs transplantation combined with ultrashort wave therapy attenuates neuroinflammation in spinal cord injury through NUR77/NF-κB pathway. *Life Sci.* **267**, 118958 (2021).
58. Führmann, T. et al. Injectable hydrogel promotes early survival of induced pluripotent stem cell-derived oligodendrocytes and attenuates longterm teratoma formation in a spinal cord injury model. *Biomaterials* **83**, 23–36 (2016).
59. Elliott Donaghue, I., Tator, C. H. & Shoichet, M. S. Local delivery of neurotrophin-3 and anti-NogoA promotes repair after spinal cord injury. *Tissue Eng. Part A* **22**(9–10), 733–741 (2016).
60. Schultz, K. R., Mona, L. R. & Cameron, R. P. Mental health and spinal cord injury: Clinical considerations for rehabilitation providers. *Curr. Phys. Med. Rehabil. Rep.* **10**(3), 131–139 (2022).

Acknowledgements

This work was supported by the National Natural Science Foundation of China grant numbers (81672173). Special orthopedic research project (Shangantong) of Sichuan Medical Association (2021SAT26). Figures 2C and D are obtained from KEGG (https://www.kegg.jp/kegg/kegg1.html) and have been reproduced with permission from Kanehisa Laboratories. Additionally, the flowchart in Fig. 6A was created using BioRender.com, and we have obtained the permission number GX277Z3XGW. We sincerely appreciate their generous assistance. We would like to extend our sincere gratitude to Dr. Xiaojun Huang for his invaluable guidance during the electrode implantation surgery. His expertise and support were instrumental in the successful execution of this procedure.

Author contributions

Kunzheng Wang conceived and designed the research. Kunzheng Wang supervised the project. Zhiping Mu, Jiaodi Qin conducted most experimental work. Jiaodi Qin, Xiaohua Zhou performed data analysis. Zhiping Mu and Jiaodi Qin wrote the manuscript. Kunzheng Wang reviewed and edited the manuscript.

Declarations

Competing interests

The authors declare no competing interests.

Ethics approval

Approval was granted by the Health Science Center of XJTU, all procedures in accordance with the Guide for the Care and Use of Laboratory Animals (NIH) and the Guidelines of the Biomedical Ethics Committee of Health Science Center of Xi'an Jiaotong University. (Exploring the Efficacy of Integrated Therapy for Spinal Cord Injury: The Promise of Combining Human Umbilical Cord Mesenchymal Stem Cells/Neural Stem Cells Transplantation with Epidural Electrical Stimulation, XJTULAE2023-1950, 1-2-2023).

Consent for publication

All authors confirm their consent for publication. The authors declare that artificial intelligence is not used in this study.

Additional information

Supplementary Information The online version contains supplementary material available at https://doi.org/10.1038/s41598-024-75754-x.

Correspondence and requests for materials should be addressed to K.W.